SANDIA REPORT

SAND97–8266 • UC–401
Unlimited Release
Printed June 1997

The Influence of Convective Heat Transfer on Flow Stability in Rotating Disk Chemical Deposition Reactors

W. S. Winters, G. H. Evans, R. Greif

Prepared by
Sandia National Laboratories
Albuquerque, New Mexico 87185 and Livermore, California 94550

Sandia is a multiprogram laboratory operated by Sandia Corporation, a Lockheed Martin Company, for the United States Department of Energy under Contract DE-AC04-94AL85000.

Sandia National Laboratories

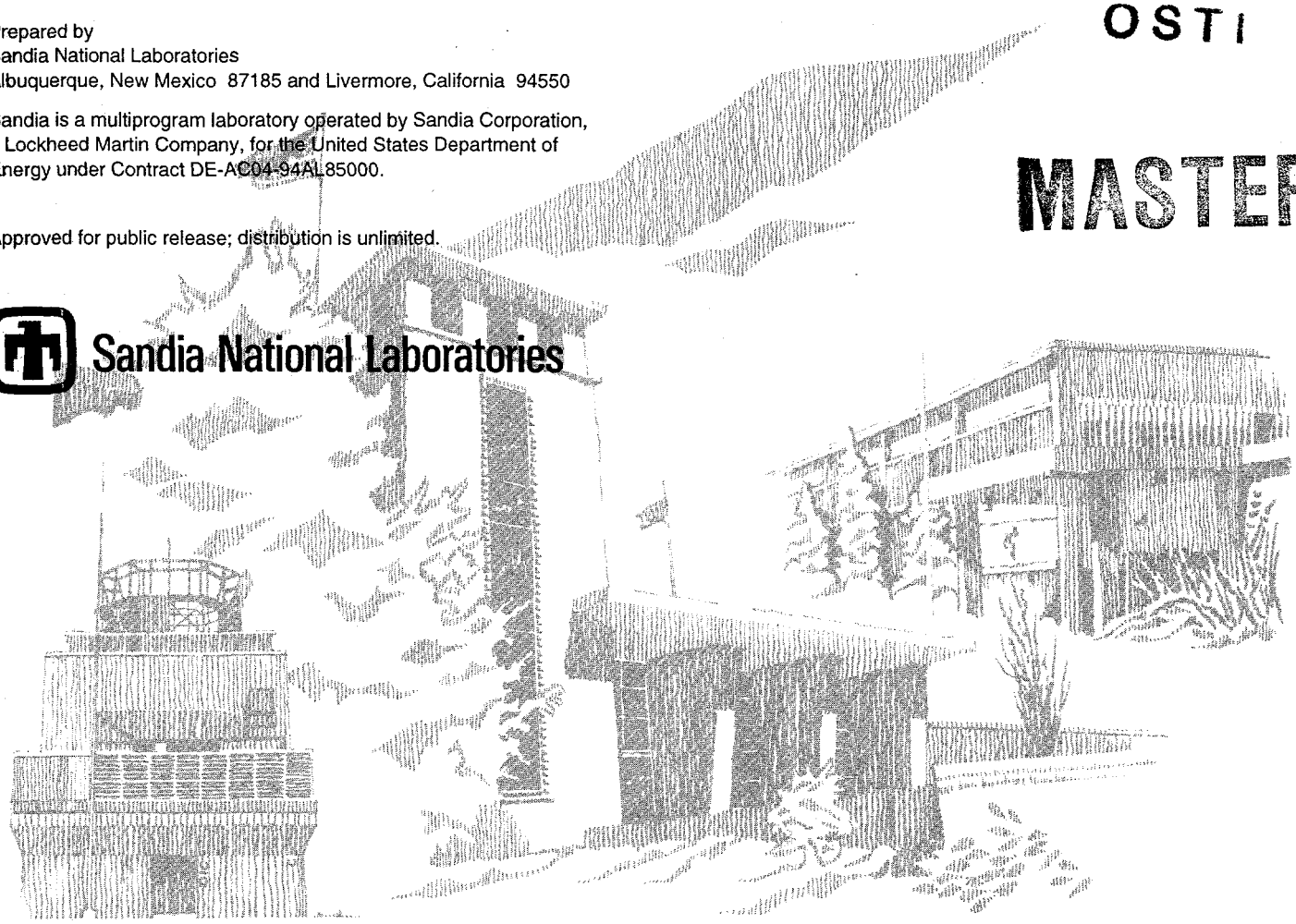

Issued by Sandia National Laboratories, operated for the United States Department of Energy by Sandia Corporation.

Available to DOE and DOE contractors from
Office of Scientific and Technical Information
P.O. Box 62
Oak Ridge, TN 37831

Prices available from (615) 576-8401, FTS 626-8401

Available to the public from
National Technical Information Service
U.S. Department of Commerce
5285 Port Royal Rd
Springfield, VA 22161

NTIS price codes
Printed copy: A03
Microfiche copy: A01

SAND97-8266
Unlimited Release
Printed June 1997

The Influence of Convective Heat Transfer on Flow Stability in Rotating Disk Chemical Vapor Deposition Reactors

W. S. Winters and G. H. Evans
Thermal and Plasma Processes Department
Sandia National Laboratories / California

R. Greif
Mechanical Engineering Department
University of California, Berkeley

The flow and heat transfer of NH_3 and He have been studied in a rotating disk system with applications to chemical vapor deposition reactors. The flow field and disk heat flux were obtained over a range of operating conditions. Comparisons of the disk convective heat transfer were made with the infinite rotating disk results to appraise uniformity of transport to the disk. Important operating variables in a rotating disk reactor include disk spin rate, disk and enclosure temperatures, flow rate, composition, pressure, and temperature of the gas mixture at the reactor inlet. These variables were studied over ranges of the primary dimensionless variables: the spin Reynolds number, Re_ω, the disk mixed convection parameter, MCP_d and a new parameter, the wall mixed convection parameter, MCP_w. Inlet velocities were set to the corresponding infinite rotating disk asymptotic velocity. Results were obtained primarily for NH_3. These results show that increasing Re_ω from 314.5 to 3145 increases the uniformity of the rotating disk heat flux and results in thinner thermal boundary layers at the disk surface. At $Re_\omega = 314.5$, increasing MCP_d to 15 leads to significant departure from the infinite disk result with nonuniform disk heat fluxes and recirculating flow patterns; the flow becomes increasingly complex at larger values of MCP_d. At the larger value of Re_ω of 3145, the results are closer to the infinite disk for MCP_d up to 15. For large negative (hot walls) and positive (cold walls) values of MCP_w, the flow recirculates and there is significant deviation from the infinite disk result; nonuniformities occur at both values of Re_ω. The influence of MCP_w on flow stability is increased at larger MCP_d and lower Re_ω. In order to determine the influence of variable transport properties (*i.e.* viscosity and thermal conductivity variation with temperature), calculations were made with He as well as NH_3; He transport property variation is low relative to NH_3. The results show that the flow of NH_3 is less stable than that of He as MCP_d is increased for $MCP_w = 0$ and $Re_\omega = 314.5$.

Contents

List of Figures

List of Tables

1 Nomenclature

A	radial aspect ratio, $\overline{r}_o/\overline{r}_d$
C	nondimensional asymptotic velocity for the infinite rotating disk (.88 for NH_3 and .79 for He; at $\overline{T}_{\rm in}$=400K and $\overline{T}_{\rm d}$=1300K)
$\mathrm{Gr_d/Re_\omega}^{3/2}$	disk mixed convection parameter, $\mathrm{MCP_d} = \overline{g}(\overline{T}_{\rm d} - \overline{T}_{\rm in})/(\overline{T}_{\rm in}\overline{\nu}_{\rm in}^{1/2}\overline{\omega}^{3/2})$
$\mathrm{Gr_w/Re_{in}}^{2}$	wall mixed convection parameter, $\mathrm{MCP_w} = \overline{g}(\overline{T}_{\rm in} - \overline{T}_{\rm w}) \cdot 2\overline{r}_o/(\overline{T}_{\rm in}\overline{u}_{\rm in}^2)$
P	pressure
Pr	Prandtl number, $\overline{c}_{p_{\rm in}}\overline{\mu}_{\rm in}/\overline{k}_{\rm in}$
$\overline{\mathrm{q}}_{\rm 1D}$	1-D infinite rotating disk heat flux (dimensional)
Re_ω	spin Reynolds number, $\overline{r}_d{}^2\overline{\omega}/\overline{\nu}_{\rm in}$
$\mathrm{Re_{in}}$	inlet Reynolds number, $2\overline{r}_o\overline{u}_{\rm in}/\overline{\nu}_{\rm in} = 2AC\sqrt{\mathrm{Re}_\omega}$
T	temperature
c_p	specific heat at constant pressure
f	ratio w/r
$\overline{g}$	acceleration of gravity (dimensional)
h	disk to inlet height
k	thermal conductivity
p_m	pressure in momentum equations
r	radial coordinate
$\overline{r}_o$	reactor radius (dimensional)
u	axial velocity component
v	radial velocity component
w	circumferential velocity component
x	axial coordinate

1.1 Greek symbols

ρ	density
ν	kinematic viscosity
μ	dynamic viscosity
ω	disk spin rate

1.2 Subscripts and superscripts

d	disk quantity
w	reactor wall quantity (for $h - H \le x \le h$, $r = A$)
$\overline{\ }$	dimensional quantity
in	evaluated at tube inlet, reference conditions
1D	one-dimensional value

2 Introduction

The uniform and controlled growth of epitaxial layers is an important step in the fabrication of microelectronic devices. The chemical vapor deposition (CVD) process is widely used for growing such layers on heated substrates that are in contact with flowing reacting gases. Control can be exerted over the deposition by specifying the composition and concentration of the gas phase species. Individual layers of materials can be deposited on a substrate by introducing active species into the gas stream in the desired sequence. Typical growth rates by CVD are on the order of microns per minute. The uniformity of layers grown by CVD often depends on the flow and heat transfer in the reactor and is effected by radiation between surfaces and convection between the gas and growth surface especially when deposition takes place near atmospheric pressure levels. CVD reactors are often designed to permit a stable, uniform and continuous flow of reacting species to the growth surface. Recirculation of the gas due to geometry and/or buoyant effects can have a strong influence on the uniformity of the heat and mass transfer and consequently the deposition.

The rotating disk reactor (RDR) takes advantage of the uniform transport properties characteristic of an infinite rotating disk in an infinite medium (see *e.g.* Evans and Greif [1]). In an infinite rotating disk flow, the heat and mass transfer to the rotating surface are said to be "ideal" in that these quantities are one-dimensional (*i.e.*, varying only with the coordinate normal to the disk). The typical RDR consists of a heated growth substrate on top of a spinning disk of finite radius oriented normal to the bulk gas flow direction. Spinning the disk minimizes circumferential deposition variations and induces a flow to the growth surface, which can lead to thinner boundary layers and improved uniformity over a larger radius. Breiland and Evans [2] have shown that RDRs can be operated under conditions where nearly ideal, one-dimensional, infinite-radius disk behavior is achieved over most of the disk surface. Deviations from the ideal flow behavior may result from the effects of variable properties, reactor geometry, gas flow rates, thermal boundary conditions, and variations in gas composition at the reactor inlet. Previous studies by Evans and Greif [3, 4], Patnaik *et al.* [5], Fotiadis *et al.* [6], and Chou and Gong [7] have examined these effects for a single component gas in a RDR. Palmateer *et al.* [8] and Winters *et al.* [9, 10] have examined convective instabilities under isothermal conditions resulting from binary gas mixing at the reactor inlet.

The present work examines, for the first time, the effects of gas properties (two gases are studied) and reactor wall temperature; a new parameter for characterizing RDR flows is introduced, namely, a wall mixed convection paramter, MCP_w. This parameter shows the dramatic effect of wall temperature on the flow stability and convection heat transfer. In addition, the effects of the large variation of the transport properties of NH_3 (a gas frequently used for depositing nitride films) is shown by comparing results obtained for He, another CVD carrier gas that has a smaller variation in properties. Results are presented in terms of common RDR flow parameters including the spin Reynolds number, Re_ω, and the disk mixed convection parameter (MCP_d). The wall mixed convection parameter, MCP_w, is varied to study the effect of reactor wall temperature on flow stability and convective heat transfer. The reactor performance is quantified by examining radial variations in the disk heat flux, normalized by the ideal infinite rotating disk heat flux.

3 Model

A cylindrical reactor of radius $\overline{r}_o$ and height $\overline{H}$ contains a spinning disk of radius $\overline{r}_d$ located a distance $\overline{h}$ from the top inlet (*cf.* Figure 1). The incoming flow consists of a single component ideal gas, either NH_3 or He, with a uniform inlet velocity, $\overline{u}_{in}$.

The dimensionless, steady, variable property, cylindrical, axisymmetric conservation equations of mass, momentum and energy for low Mach number flow, neglecting viscous dissipation and Dp/Dt (pressure work) in the energy equation, are:

$$\frac{1}{r}\frac{\partial\,(r\rho v)}{\partial r}+\frac{\partial\,(\rho u)}{\partial x}=0 \tag{1}$$

$$\frac{1}{r}\frac{\partial}{\partial r}\left(r\rho vu-\frac{r\mu}{\mathrm{Re}_\omega}\frac{\partial u}{\partial r}\right)+\frac{\partial}{\partial x}\left(\rho uu-\mu\frac{\partial u}{\partial x}\right)=-\frac{\partial p_m}{\partial x}+\frac{\mathrm{Gr_d}}{{\mathrm{Re}_\omega}^{3/2}}\frac{\rho_d}{(1-\rho_d)}(1-\rho)$$

$$+\frac{1}{r}\frac{\partial}{\partial r}\left(r\mu\frac{\partial v}{\partial x}\right)+\frac{\partial}{\partial x}\left\{\mu\frac{\partial u}{\partial x}-\frac{2\mu}{3}\left[\frac{1}{r}\frac{\partial(rv)}{\partial r}+\frac{\partial u}{\partial x}\right]\right\} \tag{2}$$

$$\frac{1}{r}\frac{\partial}{\partial r}\left(r\rho vv-\frac{r\mu}{\mathrm{Re}_\omega}\frac{\partial v}{\partial r}\right)+\frac{\partial}{\partial x}\left(\rho uv-\mu\frac{\partial v}{\partial x}\right)=-\frac{1}{\mathrm{Re}_\omega}\frac{\partial p_m}{\partial r}+r\rho f^2+\frac{1}{\mathrm{Re}_\omega}\frac{1}{r}\frac{\partial}{\partial r}\left\{r\mu\left[\frac{\partial v}{\partial r}\right.\right.$$

$$\left.\left.-\frac{2}{3}\left(\frac{1}{r}\frac{\partial(rv)}{\partial r}+\frac{\partial u}{\partial x}\right)\right]\right\}-\frac{1}{\mathrm{Re}_\omega}\frac{\mu}{r}\left\{\frac{2v}{r}-\frac{2}{3}\left[\frac{1}{r}\frac{\partial(rv)}{\partial r}+\frac{\partial u}{\partial x}\right]\right\}+\frac{1}{\mathrm{Re}_\omega}\frac{\partial}{\partial x}\left(\mu\frac{\partial u}{\partial r}\right) \tag{3}$$

$$\frac{1}{r}\frac{\partial}{\partial r}\left(r\rho vf-\frac{r\mu}{\mathrm{Re}_\omega}\frac{\partial f}{\partial r}\right)+\frac{\partial}{\partial x}\left(\rho uf-\mu\frac{\partial f}{\partial x}\right)=-\frac{2\rho vf}{r}+\frac{1}{\mathrm{Re}_\omega}\frac{2\mu}{r}\frac{\partial f}{\partial r} \tag{4}$$

$$\frac{1}{r}\frac{\partial}{\partial r}\left(r\rho vT-\frac{rk}{c_p\,\mathrm{Re}_\omega\,\mathrm{Pr}}\frac{\partial T}{\partial r}\right)+\frac{\partial}{\partial x}\left(\rho uT-\frac{k}{c_p\,\mathrm{Pr}}\frac{\partial T}{\partial x}\right)=\frac{k}{{c_p}^2\,\mathrm{Pr}}\left[\frac{1}{\mathrm{Re}_\omega}\frac{\partial T}{\partial r}\frac{\partial c_p}{\partial r}+\frac{\partial T}{\partial x}\frac{\partial c_p}{\partial x}\right] \tag{5}$$

where $f \equiv w/r$ in equation (4); u, v, w are the dimensionless axial, radial, and circumferential velocity components, respectively. The dimensionless parameters in equations (1-5) are: the disk Grashof number, $\mathrm{Gr_d} = \overline{g}(\overline{\rho}_{in}-\overline{\rho}_d)\overline{r}_d{}^3/(\overline{\rho}_d\overline{\nu}_{in}{}^2)$, the spin Reynolds number, $\mathrm{Re}_\omega = \overline{r}_d{}^2\overline{\omega}/\overline{\nu}_{in}$, and the Prandtl number, $\mathrm{Pr} = \overline{c}_{p_{in}}\overline{\mu}_{in}/\overline{k}_{in}$ ($\overline{\omega}$ is the disk spin rate; $\overline{\nu}, \overline{\mu}, \overline{\rho}, \overline{c}_p$, and $\overline{k}$ are the kinematic and dynamic viscosities, density, specific heat at constant pressure, and thermal conductivity, respectively); the properties are normalized based on their values at the temperature at the reactor inlet, $\overline{T}_{in}$. The usual scaling (Evans and Greif [3]; White [11]) for a rotating disk has been used: $\sqrt{\overline{\omega}\ \overline{\nu}_{in}}$ for the axial component of velocity, $\overline{r}_d\,\overline{\omega}$ for the radial and circumferential components of velocity, $\sqrt{\overline{\nu}_{in}/\overline{\omega}}$ for the axial coordinate, and $\overline{r}_d$ for the radial coordinate, where symbols with overbars represent dimensional quantities. The dimensionless temperature is $T = (\overline{T}-\overline{T}_{in})/(\overline{T}_d-\overline{T}_{in})$.

The boundary conditions are:

$x = 0$	$0 \le r \le 1$	$u = v = 0,\ f = T = 1$
$r = A$	$h - H \le x \le h$	$u = v = f = 0,\ T = -(\mathrm{MCP_w}/\mathrm{MCP_d})({u_{in}}^3/\mathrm{Re_{in}})$
$r = 1$	$h - H \le x \le 0$	$u = v = f = \partial T/\partial r = 0$
$r = 0$	$0 \le x \le h$	$\partial u/\partial r = \partial f/\partial r = \partial T/\partial r = v = 0$
$x = h$	$0 \le r \le A$	$v = f = T = 0,\ u = \mathrm{Re_{in}}/(2A\sqrt{\mathrm{Re}_\omega})$

where the inlet Reynolds number, $\mathrm{Re_{in}} = 2\overline{r}_o\overline{u}_{in}/\overline{\nu}_{in}$, $A = \overline{r}_o/\overline{r}_d$, and for an ideal gas, the disk Grashof number, $\mathrm{Gr_d} = \overline{g}(\overline{T}_d - \overline{T}_{in})\overline{r}_d{}^3/(\overline{T}_{in}\overline{\nu}_{in}^2)$, the wall Grashof number, $\mathrm{Gr_w} = \overline{g}(\overline{T}_{in} - \overline{T}_w)(2\overline{r}_o)^3/(\overline{T}_{in}\overline{\nu}_{in}^2)$, the disk mixed convection parameter, $\mathrm{MCP_d} = \mathrm{Gr_d}/\mathrm{Re}_\omega^{3/2}$, the wall mixed convection parameter, $\mathrm{MCP_w} = \mathrm{Gr_w}/\mathrm{Re_{in}}{}^2$. In the current study, $\mathrm{Re_{in}}$ is not an independent parameter because we consider only cases where the inlet velocity is set equal to the asymptotic velocity for an infinite rotating disk: $\overline{u}_{in} = C\sqrt{\overline{\omega}\,\overline{\nu}_{in}}$, which gives $u_{in} = C$, where C is a function of the inlet temperature, $\overline{T}_{in}$, the disk temperature $\overline{T}_d$ and the gas (see *e.g.* [3]). Thus in this study, $\mathrm{Re_{in}} = 2AC\sqrt{\mathrm{Re}_\omega}$, and the dimensionless reactor wall temperature is $T_w = -(\mathrm{MCP_w}/\mathrm{MCP_d})[C^2/(2A\sqrt{\mathrm{Re}_\omega})]$. Fully developed conditions are applied at the outflow boundary.

3.1 Numerical method

The equations are integrated over control volumes and discretized using the hybrid differencing scheme [12]. The SIMPLER method is used to determine the pressure, p_m. A sequential iterative line relaxation scheme is used to solve the equations. Underrelaxation factors (0.05-0.6) were used for the momentum and energy conservation equations; no underrelaxation was applied to the pressure equation. Iterations were continued (typically 5,000) until changes in the convective heat flux at the disk surface (the most sensitive quantity) were negligible. Computational times were one to several hours on an SGI Challenge computer. A more detailed description of the numerical method is given in reference [13].

3.2 Grid Sensitivity

All of the results discussed here were obtained on a nonuniform grid of 80 by 40 control volumes in the x and r directions, respectively, between the inlet and the disk, with finer grid spacings near the rotating disk ($x = 0$). The control volumes were distributed over three computational regions (one bounded by the inlet and the disk, a second adjacent to the first bounded by the inlet and the beginning of the annular exit, and a third for the annular exit). A nonuniform grid of 25 by 10 control volumes in the x and r directions was used for the annular exit. Calculations were also made on a nonuniform x, r grid of 50 by 40 control volumes above the disk. Results for the disk heat flux differed by less than 5% for the two grid distributions. Furthermore, the fine grid resolution of the rotating disk boundary layer was deemed adequate because the results of the numerical calculations at the centerline ($r = 0$) differed from the similarity solution [14] for the flow over an infinite rotating disk by less than 2%. Deviations greater than 2% tended to occur only at the edges of

the disk unless buoyancy or the development of sidewall boundary layers disturbed the "one-dimensional" nature of the heat flux over the disk.

4 Results and Discussion

Results were obtained for the system shown in Figure 1. This system is representative of typical RDR's and is similar, if not identical to, geometries studied previously in [3, 4, 9, 10]. Results are presented using the dimensionless groups defined in the previous sections, *i.e.* the spin Reynolds number, $\mathrm{Re}_\omega = \overline{r}_d{}^2\overline{\omega}/\overline{\nu}_{\mathrm{in}}$, the disk mixed convection parameter, $\mathrm{MCP_d} = \mathrm{Gr_d}/\mathrm{Re}_\omega{}^{3/2}$, and a new parameter for characterizing RDR flows, the wall mixed convection parameter, $\mathrm{MCP_w} = \mathrm{Gr_w}/\mathrm{Re_{in}}{}^2$. A fourth parameter, the inlet Reynolds number, $\mathrm{Re_{in}} = 2\overline{r}_o\overline{u}_{\mathrm{in}}/\overline{\nu}_{\mathrm{in}}$, normally an independent parameter, is not independent in this study because the inlet velocity was selected to be the "natural drawing velocity" computed from the infinite rotating disk solution [14] for the same operating conditions. Under these circumstances, it can be shown that $\mathrm{Re_{in}}$ is directly related to Re_ω (see Section 3). Variations in another independent parameter, the Prandtl number, Pr, were not considered since the Prandtl numbers for common carrier gases in RDRs are nearly equal (*cf.* Table 1). This study also presents new results for the effects of variable properties by considering two common CVD gases, NH_3 and He. Results were obtained for two spin Reynolds numbers which span a range characteristic of RDRs: $\mathrm{Re}_\omega = 314.5$ and $\mathrm{Re}_\omega = 3145.$. For each spin Reynolds number, $\mathrm{MCP_d}$ was increased from nearly zero to a level where significant departure from the ideal infinite rotating disk behavior was obtained. The wall mixed convection parameter, $\mathrm{MCP_w}$, was varied from -30 to $+30$; negative values are for hotter walls relative to the inlet while positive values are for cooler walls relative to the inlet.

4.1 The Ideal Reactor

While stable reactor flows are not always "sufficient" to produce uniform CVD, flow stability and uniformity are often "necessary" for many processes. One measure of reactor flow suitability is how well the disk heat flux compares to the corresponding "ideal" infinite rotating disk heat flux, $\overline{q}_{1\mathrm{D}}$ which is defined as:

$$\overline{q}_{1\mathrm{D}} = \left[-\overline{k}\,\frac{\partial \overline{T}}{\partial \overline{x}}\bigg|_{\overline{x}=0} \right]_{1\mathrm{D}} \tag{6}$$

Because RDRs have finite disk diameters, deviation from the ideal flow is unavoidable at the disk edges due to two-dimensional effects. For geometries like the one shown in Figure 1, the disk heat flux usually exceeds the ideal value at the disk edges due the local flow acceleration which accompanies the flow into the narrow exit channel. However, under stable operating conditions, it is reasonable to expect the RDR flow to approximate the ideal flow over a large portion of the disk.

Figure 2 illustrates reactor flow (NH_3) characteristics for $\mathrm{Re}_\omega = 314.5$, $\mathrm{MCP_d} = 1.3$, and $\mathrm{MCP_w} = 0$ (equal wall and inlet temperatures). The figure is typical of how the flow field results will be presented in this report. Figure 2 (a) shows the reactor in cross-section with white streamlines superimposed over color filled temperature contours. Blue corresponds to the lowest temperature (inlet and cold walls) and red corresponds to the highest temperature (disk) in the flow field. A more detailed legend of contour values will not be presented because these plots are intended to demonstrate the qualitative nature of the flow even though the plots were generated from computed results. More quantitative information is presented in Figure 2 (b)

shows the heat flux distribution along the disk surface. The radial position is normalized by the disk radius (9 cm) and the heat flux is normalized by the ideal infinite rotating disk heat flux ($3.37 \times 10^6 ergs/s - cm^2$) which was computed from the similarity solution [1] using the computer code SPIN [14]. SPIN calculations account for property variations due to temperature. Both SPIN and the two-dimensional computational model utilize CHEMKIN transport models [15] for determining thermodynamic and transport properties of ideal gas mixtures.

The normalized heat flux plot of Figure 2 (b) shows excellent agreement between the 2-D model and the 1-D result over 60% of the disk radius. Figure 3 (a) compares the centerline (r=0) temperature distributions computed from the two results. The distributions are almost identical. The plot shows a thermal boundary layer thickness of approximately 6 cm above the disk. The boundary layer can also be seen in the color-filled temperature contour plot of Figure 2 (a). The centerline (r=0) axial component of velocity for the two results is shown in Figure 3 (b). Agreement is excellent in the boundary layer and at the reactor inlet. However, the 2-D model predicts an accelerating flow that reaches a maximum approximately 10 cm above the disk. This acceleration is caused by the formation of a momentum boundary layer on the vertical walls of the reactor. This boundary layer is evident from the curvature of the streamlines along the vertical walls in Figure 2 (a). Despite the effects noted near the disk, the 2-D flow retains the 1-D behavior.

The effect of increasing the spin Reynolds number by a factor of 10 is shown in Figures 4 and 5. The mixed convection parameters were unchanged ($MCP_d = 1.3$ and $MCP_w = 0$) and the gas was NH_3. Note that $\overline{u}_{in}$, the dimensional inlet velocity, is smaller for the larger Re_ω. This occurs because MCP_d is kept constant at 1.3 for both Re_ω and Re_ω was increase by increasing $\overline{\omega}$, increasing $\overline{P}$, and decreasing $\overline{u}_{in}$. Increasing Re_ω increases the induced flow rate due to the rotating disk. This results in a thinner thermal boundary layer adjacent to the disk (Figure 4 (a) compared to Figure 2 (a)) and increases the disk heat flux. Heat flux uniformity has also improved. Figure 4 (b) shows that the heat flux is in excellent agreement with the 1-D result over approximately 90% of the disk radius. The thinner boundary layer (approximately 2 cm) is evident in Figure 5 which compares the centerline (r=0) axial component of velocity and temperature profiles with the 1-D results.

4.2 The Influences of MCP_d and Re_ω

Results presented in this section are for cases where $MCP_w = 0$ (equal inlet and wall temperatures). All calculations were performed for NH_3. Figure 6 shows reactor behavior over a wide range of values of MCP_d for the low spin Reynolds number ($Re_\omega = 314.5$). The flow retains its nearly 1-D appearance until the disk mixed convection parameter is increased beyond 10. At $MCP_d = 15$ there is a strong but steady recirculating pattern that decreases the disk boundary layer thickness near the centerline but increases it near the outer edges of the disk. The influence of the value of MCP_d on disk heat flux is illustrated in Figure 7. For $MCP_d = 5$ the heat transfer retains the 1-D nature discussed in the previous section (for $MCP_d = 1.3$). At $MCP_d = 10$, some departure from the 1-D behavior is apparent; the magnitude has increased slightly but

the distribution remains relatively uniform. At $MCP_d = 15$ there is a recirculating flow that affects both the magnitude and uniformity of the disk heat flux. Further increases in MCP_d cause stronger recirculations and correspondingly greater departure from the 1-D heat flux result.

Figure 8 shows flow and heat transfer behavior with varying MCP_d at the high spin Reynolds number ($Re_\omega = 3145$). Increasing the spin Reynolds number by a factor of 10 results in a decreased thermal boundary layer thickness and a corresponding increase in the disk heat transfer as discussed in Section 4.1. Here again, the flow retains its nearly 1-D appearance until the disk mixed convection parameter is increased to 10. The effect of the departure from ideal flow is seen in Figure 9. For $MCP_d = 10$, the heat flux near the centerline shows a slight increase (2 %) above the 1-D result. Heat flux uniformity is also affected. Increases in the disk MCP beyond 15 are likely to produce even greater departures from the 1-D behavior. However, the steady recirculating flow patterns observed for $MCP_d > 10$ and $Re_\omega = 314.5$ (see *e.g.* Figure 6 (c-d)) could not be verified for $Re_\omega = 3145$ because the flow became unsteady and convergence to a steady result was not obtained.

4.3 The Influence of MCP_w and Re_ω

In order to determine the influence of wall temperature on reactor flow and heat transfer, the wall mixed convection parameter, MCP_w, was varied over a range typical for RDRs. The disk mixed convection parameter, MCP_d was fixed at 5 and results were obtained for NH_3 at the two spin Reynolds numbers (314.5 and 3145). Figure 10 shows reactor temperature contours and streamlines for $MCP_w = -30, -10, 0, +10, +30$ for a spin Reynolds number of 314.5. The corresponding disk heat flux profiles are shown in Figure 11. For $MCP_w = -30$, the wall is hotter than the downward flowing gas, and a buoyancy induced recirculation develops near the reactor walls. This causes the downward flow to be channeled inward toward the reactor centerline; note the inward curvature of the streamlines in Figure 10 (a). This results in a slight increase in the disk heat transfer over the entire disk (Figure 11). Cooling the walls relative to the inlet ($MCP_w = +10$), provides an additional downward flow force which acts to thin the boundary layer near the wall and eliminates the potential buoyant instability which occurs for hot walls (negative values of MCP_w). This results in a slight decrease in the disk heat transfer over the outer part of the disk. Further cooling of the wall ($MCP_w = +30$) intensifies the downward sidewall flow to the point where a weak recirculation develops causing the heat transfer to become nonuniform and reduced over the outer half of the disk.

Figure 12 shows reactor temperature contours and streamlines for $MCP_w = -30, -10, 0, +10, +30$ at the higher spin Reynolds number of 3145 and the same MCP_d value of 5. The corresponding disk heat flux profiles are shown in Figure 13. For $MCP_w = -30$, the buoyancy induced recirculation that develops near the reactor walls is stronger than for the lower spin Reynolds number. However the resulting departure from the 1-D heat flux is less. Side wall cooling ($MCP_w > 0$) induces a downward flow near the walls which is strong enough to draw the flow away from the center causing an outward bending of the streamlines approximately 4 cm above the disk. This flow redirection results in heat flux nonuniformity near the outer

Carrier Gas	$\frac{k_{1300}}{k_{400}}$	$\frac{\mu_{1300}}{\mu_{400}}$	Pr_{400}	Pr_{1300}
NH_3	4.75	2.99	.72	.73
H_2	2.35	2.15	.69	.69
He	2.14	2.15	.67	.67
N_2	2.58	2.21	.71	.71
O_2	2.64	2.23	.71	.71
Ar	2.28	2.28	.67	.67

Note: Subscripts indicate properties evaluated at 400 K and 1300 K.

Table 1: Properties for Common CVD Carrier Gases.

edge of the disk. Here again, the departure from the 1-D result is less than that observed for the lower spin Reynolds number. At higher values of MCP_d, variations in MCP_w lead to greater departures from the 1-D behavior. Figure 14 shows the results for MCP_w of $-30, 0, +30$ at $MCP_d = 7$ and $Re_\omega = 3145$. The small increase in MCP_d from 5 to 7 results in a substantial increase in disk heat flux nonuniformity. Further increases in MCP_d lead to unsteady flows for $MCP_w = +30$.

4.4 The Influence of Variable Gas Properties

Table 1 shows transport property and Prandtl number variations for common RDR gases evaluated at 400 and 1300 K. These values were obtained from reference [16]. Prandtl numbers for the common carrier gases are nearly equal and constant over the temperature range considered here. Hence, if it could be shown that variations of the transport properties with temperature are unimportant, the results presented in the previous sections apply for all the common carrier gases.

To determine the influence of variable transport properties, several calculations were repeated using He in place of NH_3. Note that the largest variation in transport properties for the gases shown in Table 1 occurs for NH_3, the least for He. Figure 15 shows flow and temperature fields and disk heat flux profiles for He and NH_3 at a spin Reynolds number of 314.5 and for disk mixed convection parameters of 10 and 15. In all cases $MCP_w = 0$ and the inlet velocity was set equal to the infinite rotating disk asymptotic velocity result for the particular gas (NH_3 or He). Using the asymptotic velocity caused Re_{in} for the NH_3 and He calculations to be slightly different (47 for NH_3 and 42 for He). Results at $MCP_d = 10$ show 1-D behavior for both He and NH_3. However, the variable transport properties for NH_3 have caused the thermal boundary layer to be nearly twice that of He. This is evident from the color filled temperature contours in Figure 15

(a). This trend was also observed for all calculations made at $MCP_d < 10$ (results not shown here). At $MCP_d = 15$ NH_3 exhibits a significant departure from 1-D flow with nonuniform heat transfer and strong recirculating flow. In contrast, the He flow resembles the 1-D result with only a slight nonuniformity in the disk heat flux.

5 Conclusions

The flow and heat transfer of NH_3 and He have been studied for a typical RDR geometry. The study extends earlier results by determining the important effects of reactor wall temperature and variable gas properties on flow stability and convective heat transfer. The parameters that were varied are the spin Reynolds number, Re_ω, the disk mixed convection parameter, MCP_d, and a new parameter, the wall mixed convection parameter, MCP_w. The inlet Reynolds number, Re_{in} was varied so that the inlet velocity was equal to the asymptotic velocity for the corresponding infinite rotating disk (*ie.* the "unstarved" flow case). The influence of variable transport properties was investigated by comparing results for He and NH_3.

The results for NH_3 show that increasing Re_ω from 314.5 to 3145 increases the uniformity of the rotating disk heat flux and results in thinner thermal boundary layers at the disk surface. At Re_ω= 314.5, increasing MCP_d to 15 leads to significant departure from the 1-D infinite disk result with nonuniform disk heat fluxes and recirculating flow patterns; the flow becomes increasingly complex at larger values of MCP_d. At the larger value of Re_ω of 3145, the results are closer to the 1-D infinite disk for MCP_d up to 15. However, at the larger Re_ω, steady results could not be obtained for values of $MCP_d > 15$, whereas steady, recirculating flow results were obtained for $MCP_d > 15$ at the smaller Re_ω.

For large negative (hot walls) and positive (cold walls) values of MCP_w, the flow recirculates and there is significant deviation from the one-dimensional result; the nonuniformities occur at both the small and the large Re_ω. The sensitivity to large variations in MCP_w is increased at larger MCP_d and lower Re_ω.

Substituting He for NH_3 for several calculations demonstrated the strong influence due to the variable transport properties. For He (smaller variation in transport properties), the disk thermal boundary layers tended to be thinner and the flow was more stable over a larger range of MCP_d.

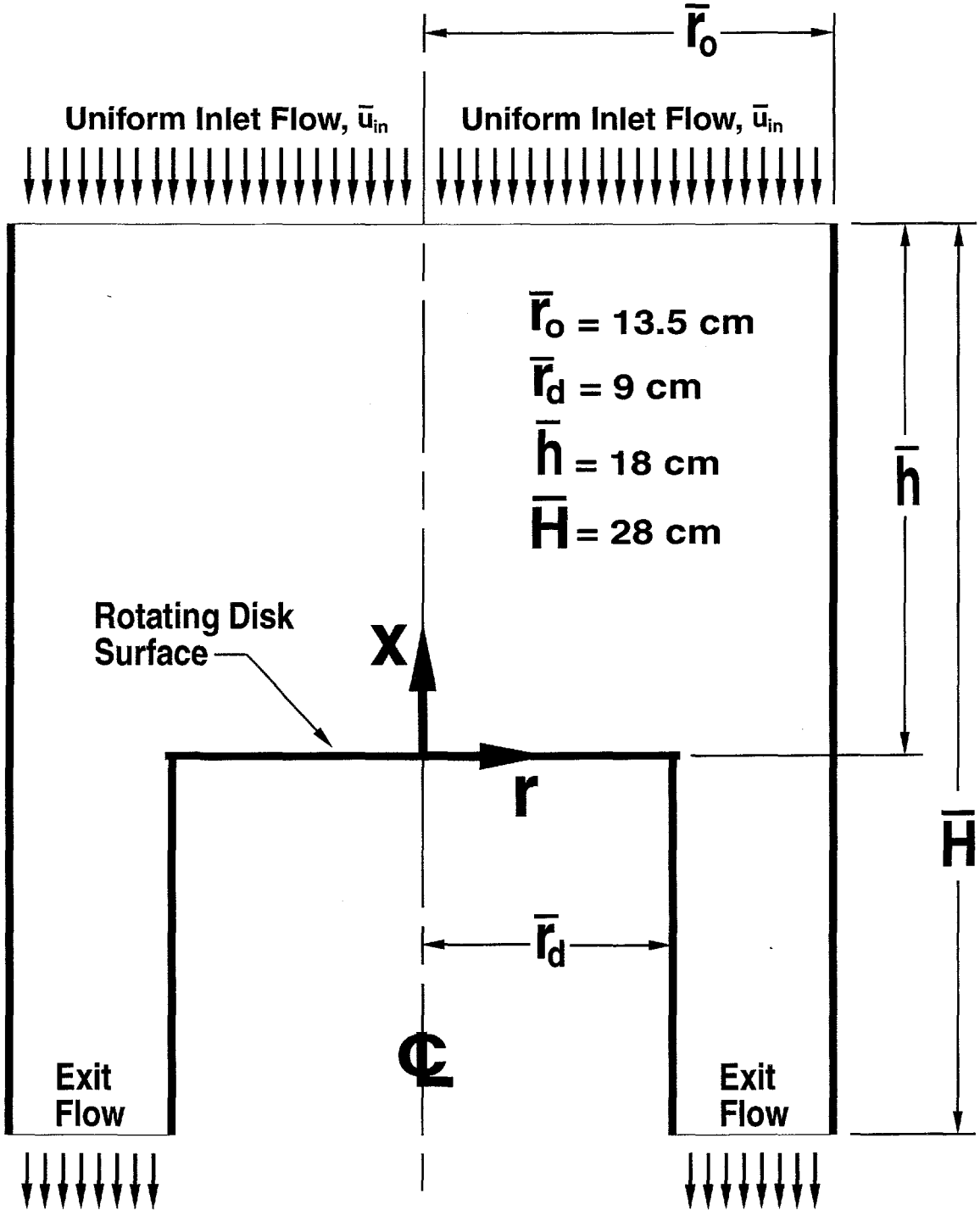

Figure 1: Reactor geometry.

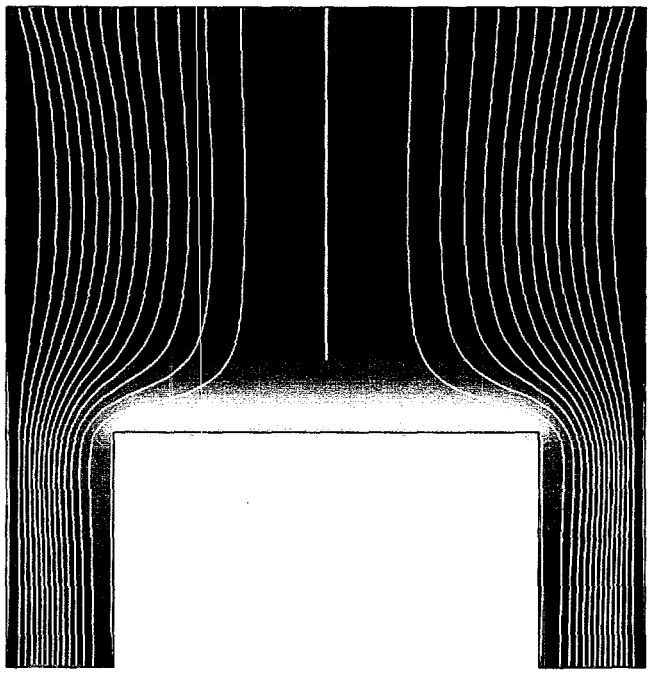

(a) Color fill temperature contours (blue=cold, red=hot) with superimposed streamlines.

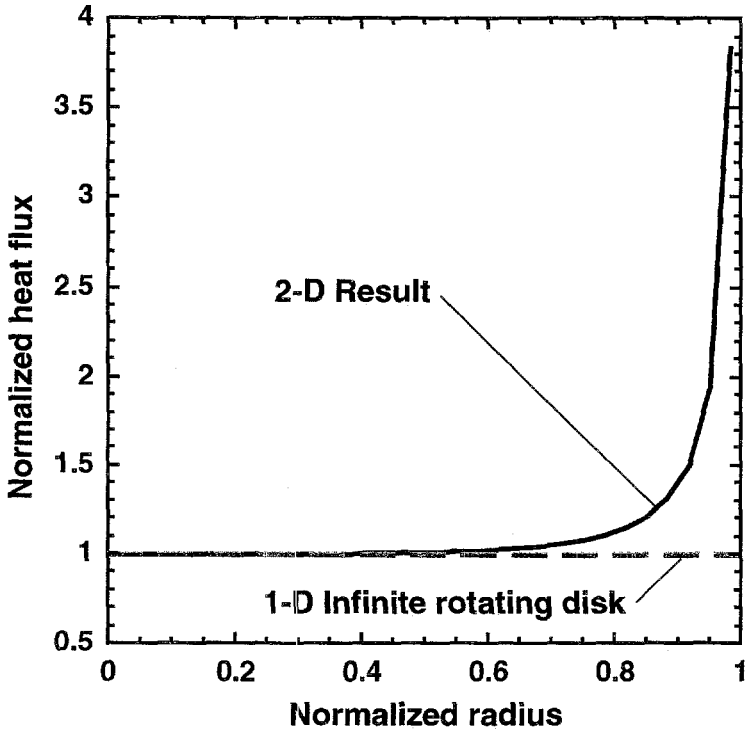

(b) Disk heat flux distribution

Figure 2: Comparison with 1-D infinite rotating disk solution for $\mathrm{Re}_\omega = 314.5$, $\mathrm{MCP_d} = 1.3$, and $\mathrm{MCP_w} = 0$. Conditions: 13.5 torr, 562 RPM, $\overline{\mathrm{T}}_\mathrm{d} = 1300\mathrm{K}$, $\overline{\mathrm{T}}_\mathrm{in} = 400\mathrm{K}$, $\overline{\mathrm{T}}_\mathrm{w} = 400\mathrm{K}$, $-\overline{u}_\mathrm{in} = 26.3\mathrm{cm/sec}$, and $\overline{\mathrm{q}}_\mathrm{1D} = 3.37 \times 10^6 \mathrm{ergs/sec} - \mathrm{cm}^2$.

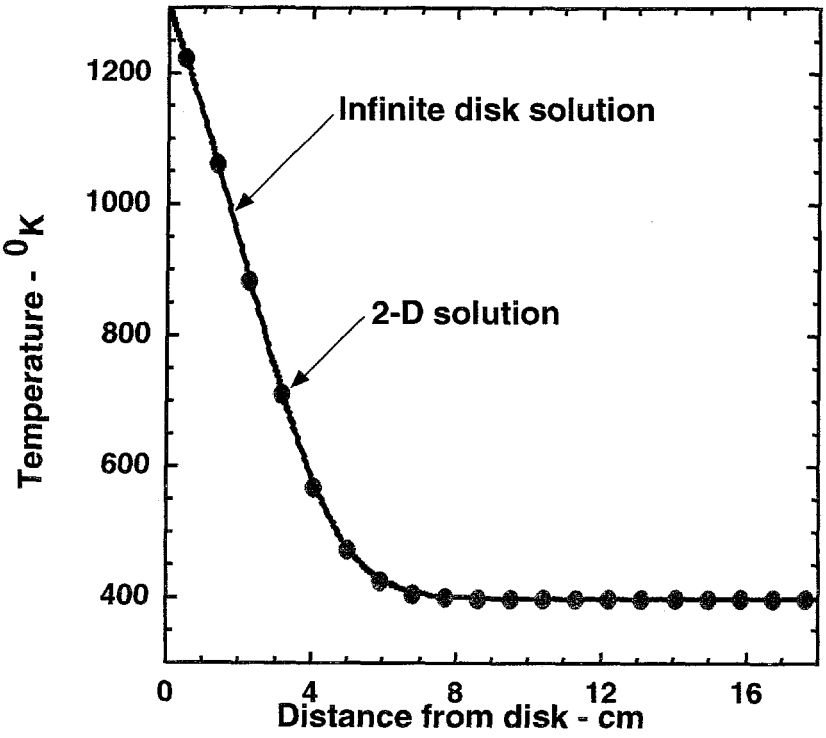

(a) Centerline temperature distribution

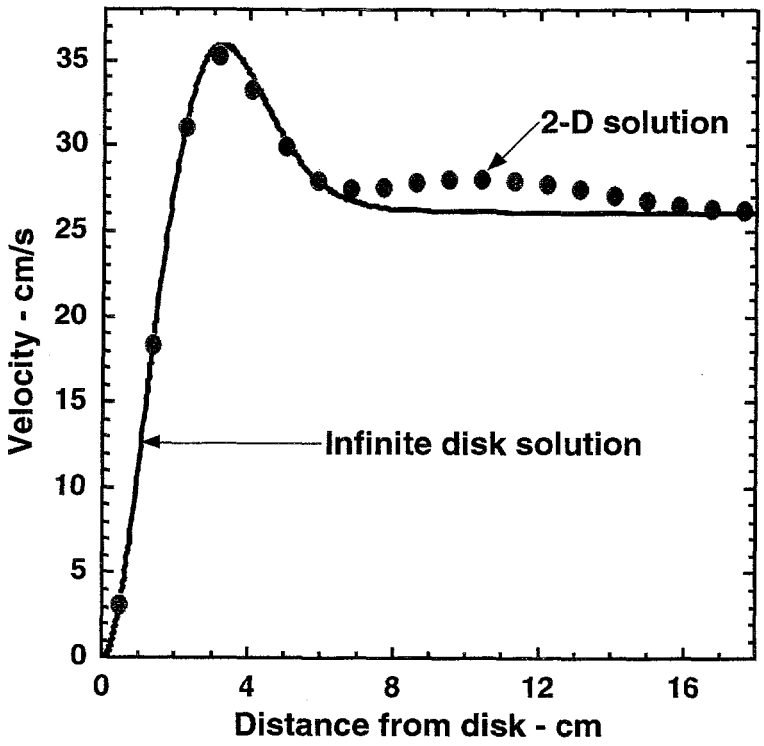

(a) Centerline velocity distribution

Figure 3: Comparison of 1-D and 2-D centerline (r=0) profiles for $Re_\omega = 314.5$, $MCP_d = 1.3$, and $MCP_w = 0$. Conditions: 13.5 torr, 562 RPM, $\overline{T}_d = 1300K$, $\overline{T}_{in} = 400K$, $\overline{T}_w = 400K$, $-\overline{u}_{in} = 26.3cm/sec$, and $\overline{q}_{1D} = 3.37 \times 10^6 ergs/sec - cm^2$.

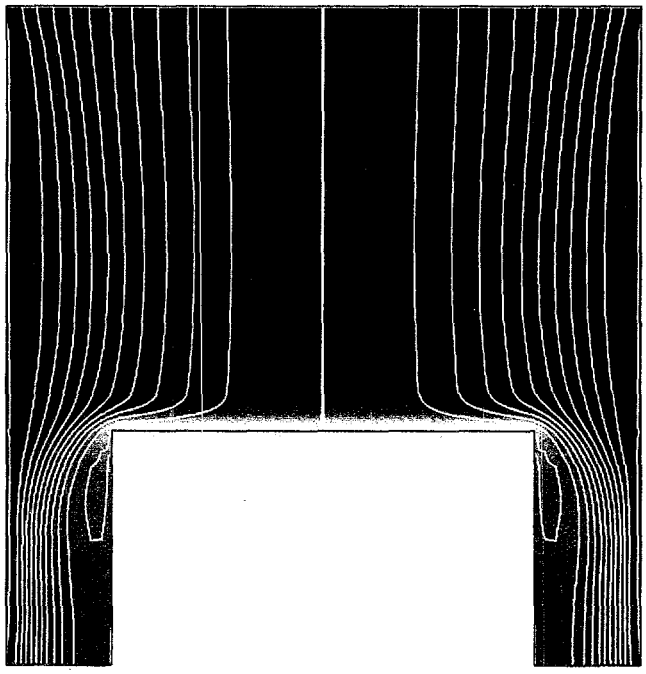

(a) Color fill temperature contours (blue=cold, red=hot) with superimposed streamlines.

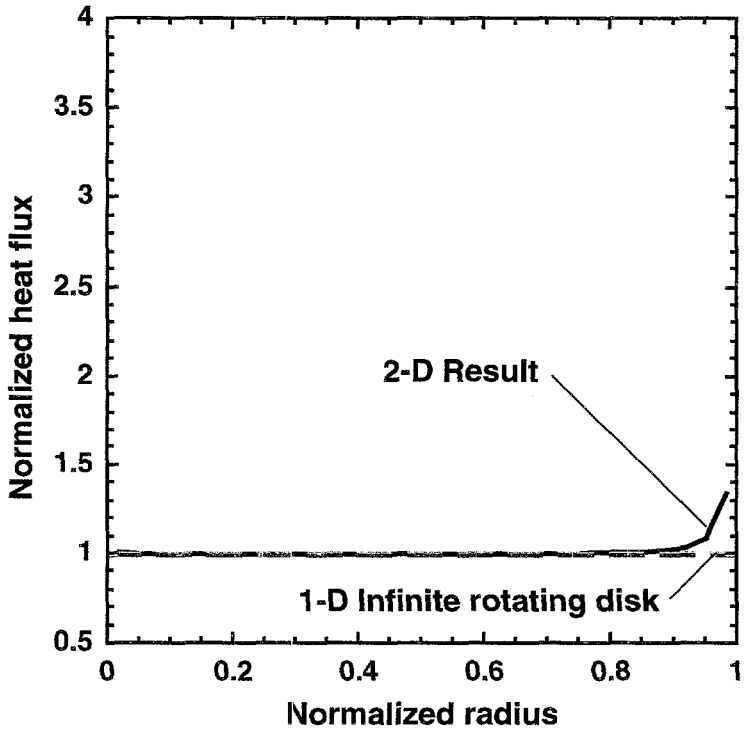

(b) Disk heat flux distribution

Figure 4: Comparison with 1-D infinite rotating disk solution for $Re_\omega = 3145$, $MCP_d = 1.3$, and $MCP_w = 0$. Conditions: 76 torr, 1000 RPM, $\overline{T}_d = 1300K$, $\overline{T}_{in} = 400K$, $\overline{T}_w = 400K$, $-\overline{u}_{in} = 14.8cm/sec$, and $\overline{q}_{1D} = 1.07 \times 10^7 ergs/sec - cm^2$.

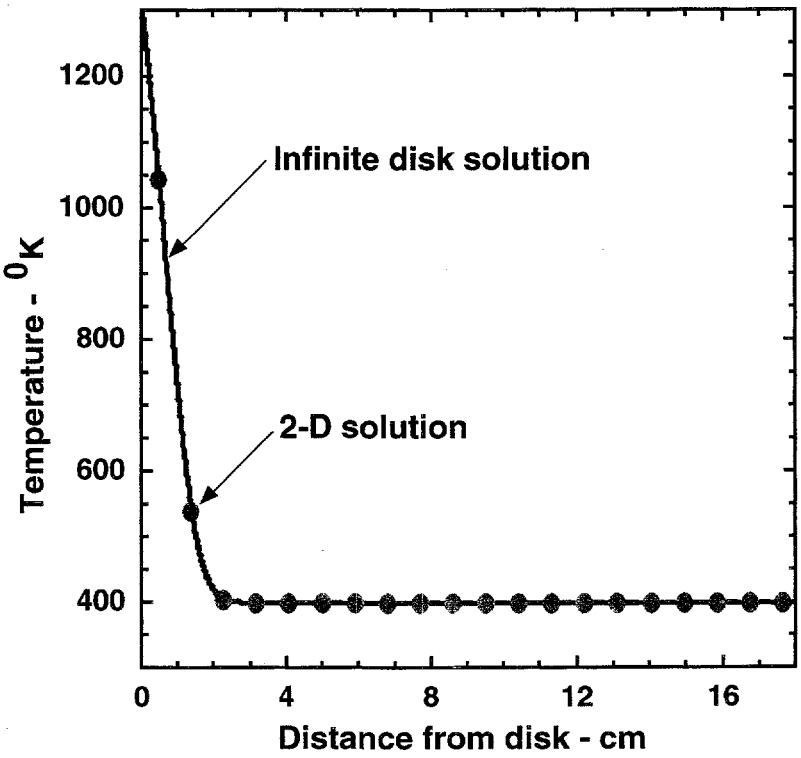

(a) Centerline temperature distribution

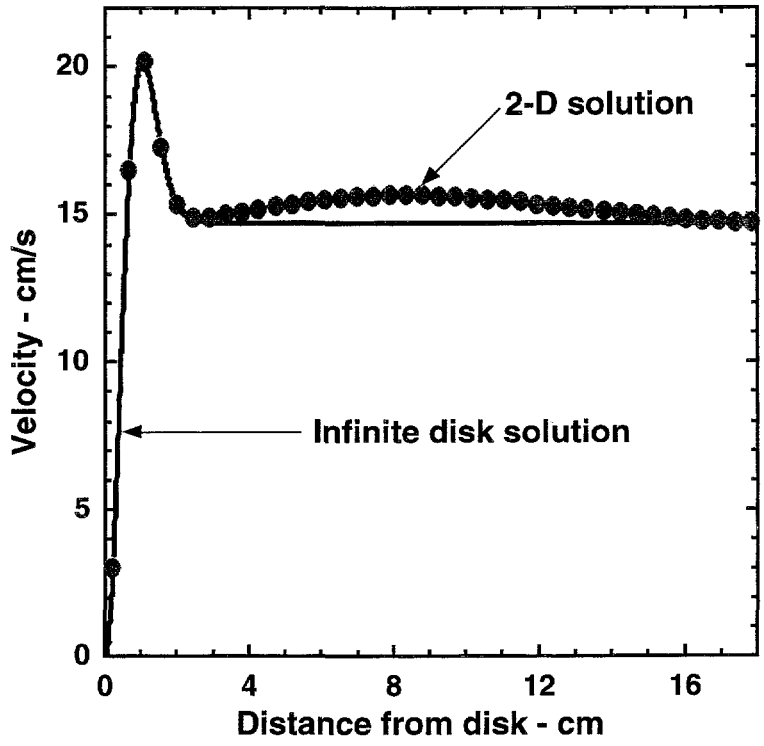

(a) Centerline velocity distribution

Figure 5: Comparison of 1-D and 2-D centerline (r=0) profiles for $Re_\omega = 3145$, $MCP_d = 1.3$, and $MCP_w = 0$. Conditions: 76 torr, 1000 RPM, $\overline{T}_d = 1300K$, $\overline{T}_{in} = 400K$, $\overline{T}_w = 400K$, $-\overline{u}_{in} = 14.8cm/sec$, and $\overline{q}_{1D} = 1.07 \times 10^7 ergs/sec - cm^2$.

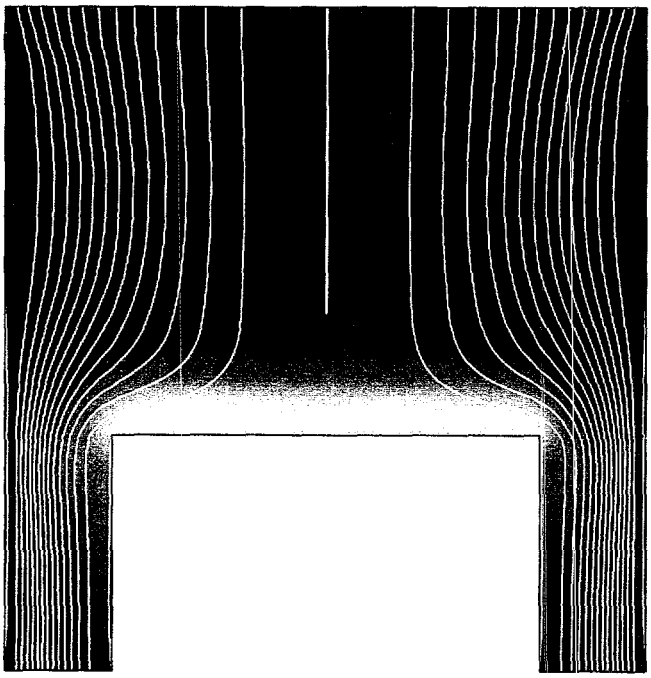

(a) Disk MCP=5

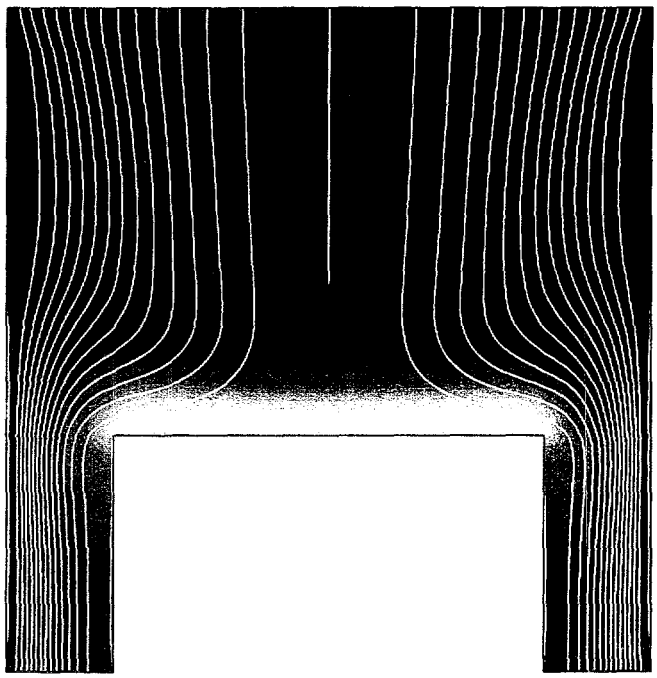

(b) Disk MCP=10

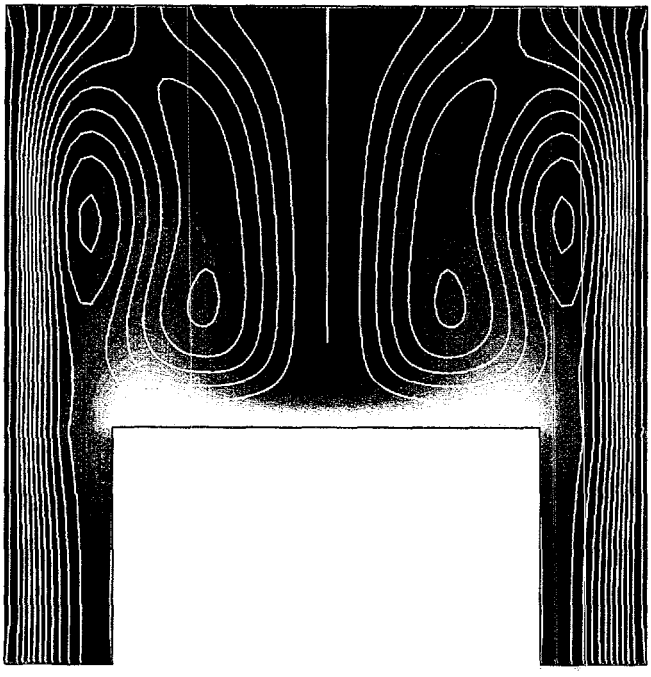

(c) Disk MCP=15

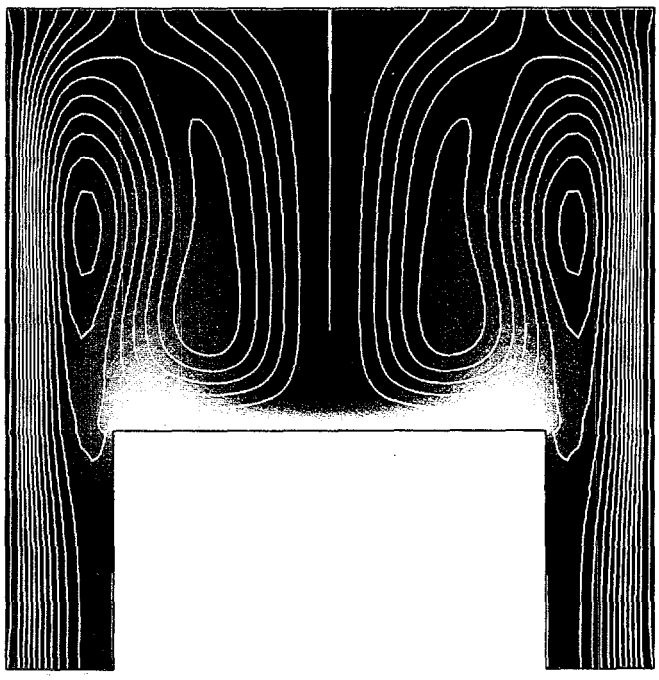

(d) Disk MCP=20

Figure 6: Influence of MCP_d on flow and temperature at $Re_\omega = 314.5$. Conditions: $\overline{T}_d = 1300, K$, $\overline{T}_{in} = 400K$, $\overline{T}_w = 400K$, and $\overline{q}_{1D} = 3.37 \times 10^6 ergs/sec - cm^2$; (a) 27 torr, 281 RPM,$-\overline{u}_{in} = 13.2cm/sec$, (b) 38 torr, 198 RPM,$-\overline{u}_{in} = 9.3cm/sec$, (c) 47 torr, 162 RPM,$-\overline{u}_{in} = 7.6cm/sec$, (d) 54 torr, 141 RPM,$-\overline{u}_{in} = 6.6cm/sec$.

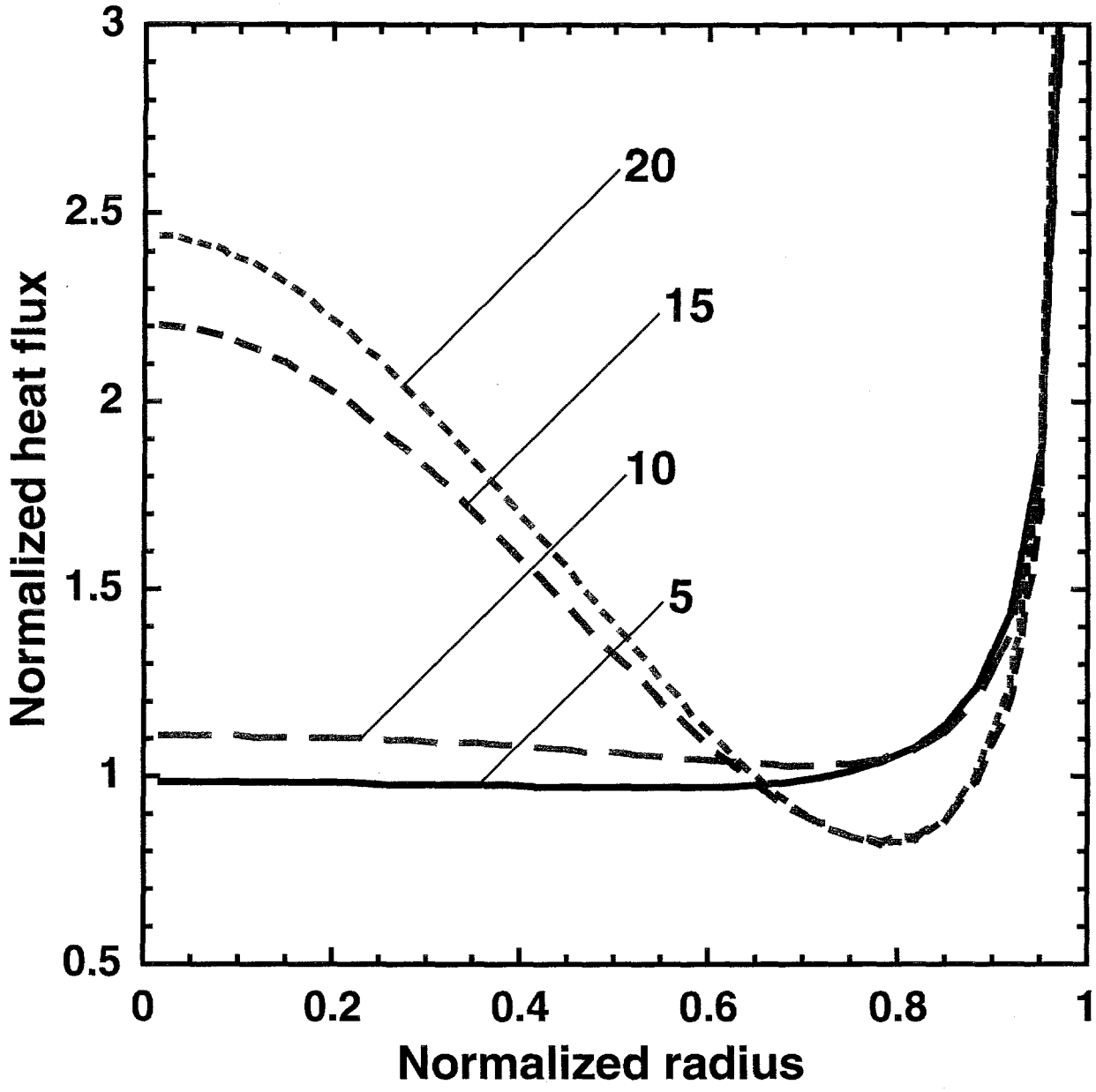

Figure 7: Influence of MCP_d on disk heat flux at $Re_\omega = 314.5$. Conditions: $\overline{T}_d = 1300K$, $\overline{T}_{in} = 400K$, $\overline{T}_w = 400K$, and $\overline{q}_{1D} = 3.37 \times 10^6 ergs/sec - cm^2$; $MCP_d = 5$: 27 torr, 281 RPM, $-\overline{u}_{in} = 13.2cm/sec$, $MCP_d = 10$: 38 torr, 198 RPM,$-\overline{u}_{in} = 9.3cm/sec$, $MCP_d = 15$: 47 torr, 162 RPM,$-\overline{u}_{in} = 7.6cm/sec$, $MCP_d = 20$: 54 torr, 141 RPM,$-\overline{u}_{in} = 6.6cm/sec$.

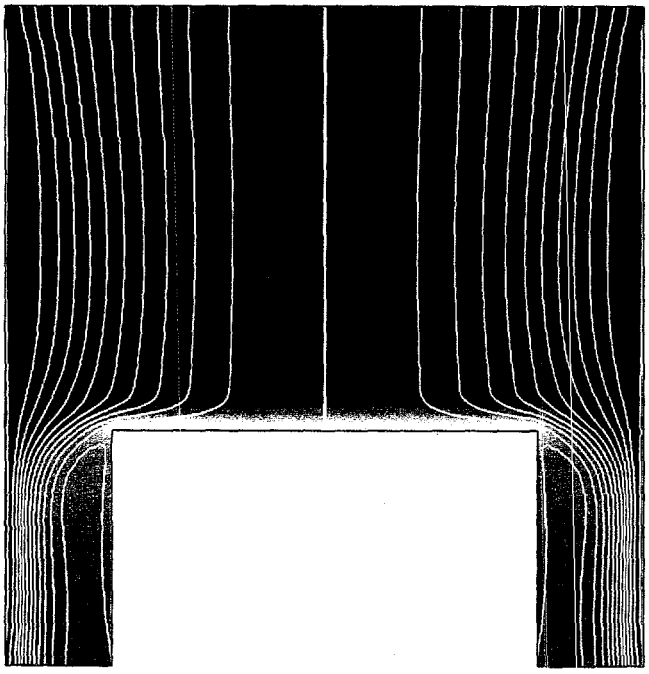

(a) Disk MCP=5

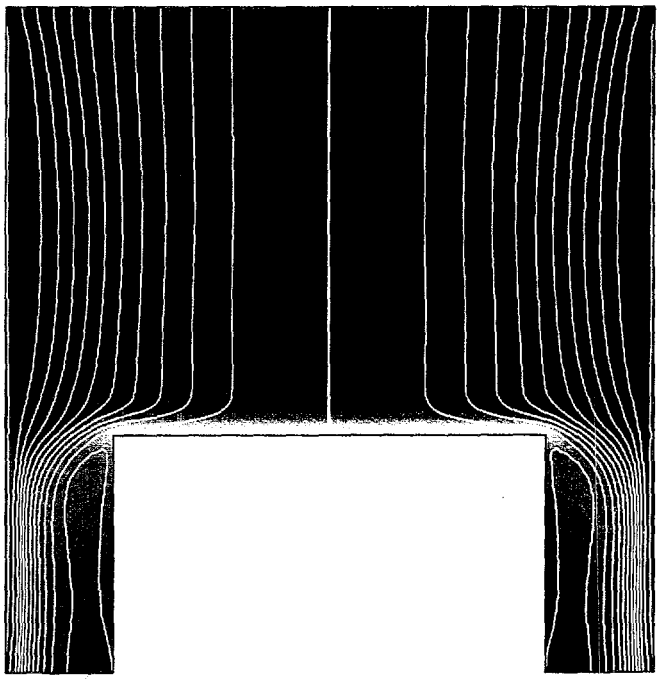

(b) Disk MCP=7

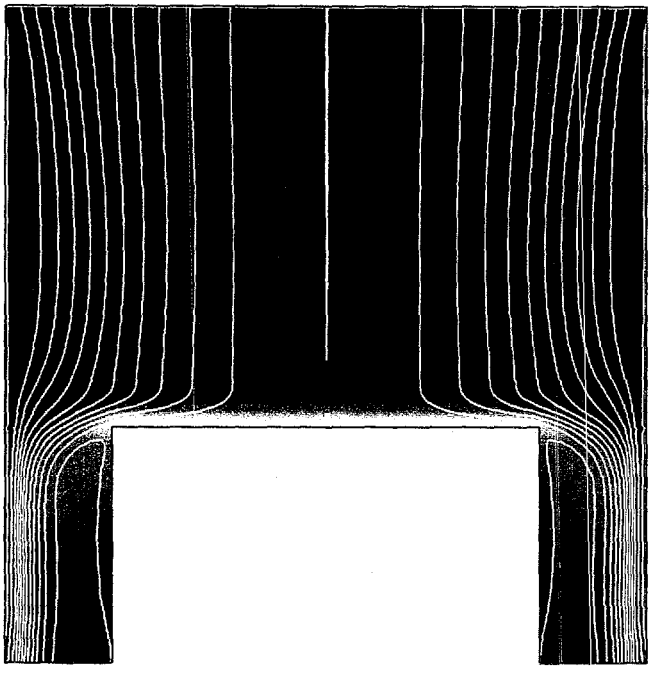

(c) Disk MCP=10

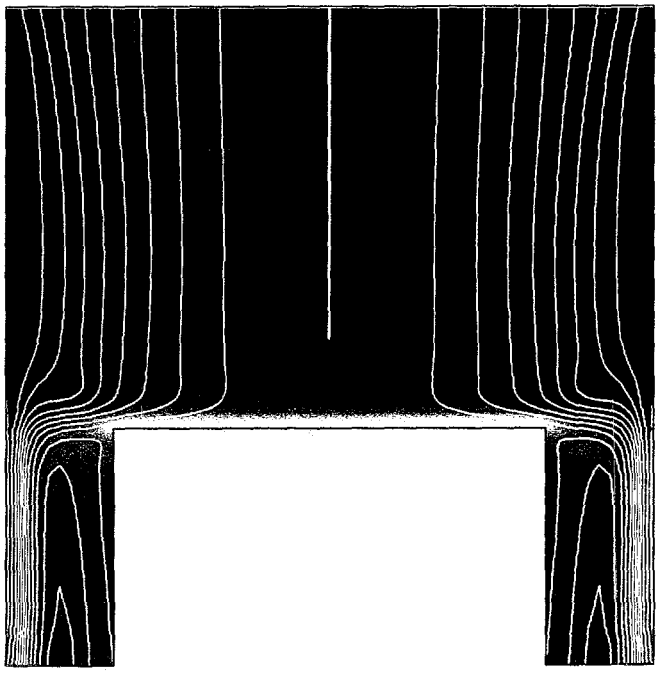

(d) Disk MCP=15

Figure 8: Influence of MCP_d on flow and temperature at $Re_\omega = 3145$. Conditions: $\overline{T}_d = 1300K$, $\overline{T}_{in} = 400K$, $\overline{T}_w = 400K$, and $_{1D} = 1.07 \times 10^7 ergs/sec - cm^2$; (a) 152 torr, 500 RPM,$-\overline{u}_{in} = 7.4cm/sec$, (b) 180 torr, 423 RPM,$-\overline{u}_{in} = 6.3cm/sec$, (c) 215 torr, 354 RPM,$-\overline{u}_{in} = 5.2cm/sec$, (d) 263 torr, 289 RPM,$-\overline{u}_{in} = 4.3cm/sec$.

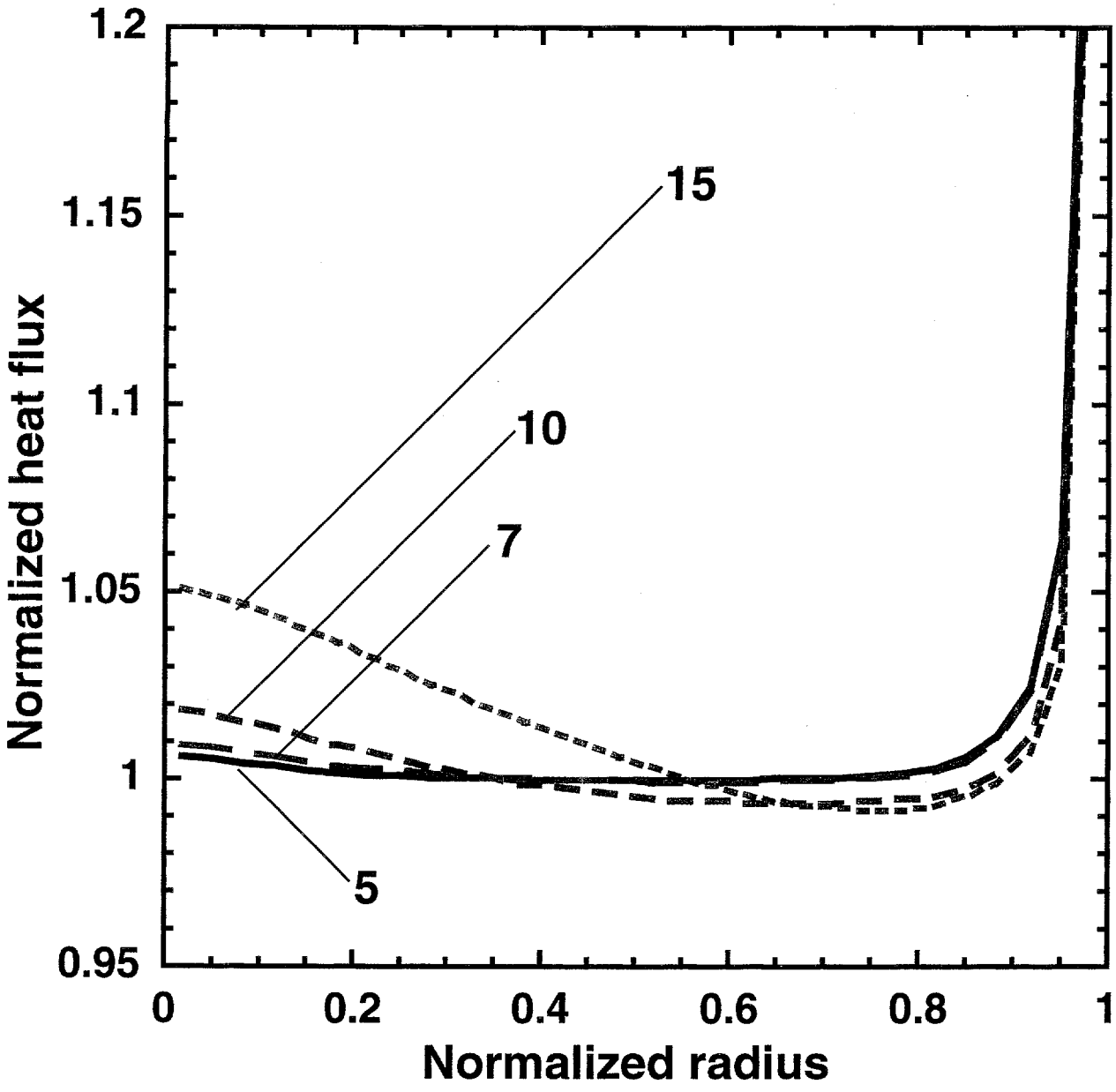

Figure 9: Influence of MCP_d on disk heat flux at $Re_\omega = 3145$. Conditions: $\overline{T}_d = 1300K$, $\overline{T}_{in} = 400K$, $\overline{T}_w = 400K$, and $\overline{q}_{1D} = 1.07 \times 10^7 ergs/sec - cm^2$; $MCP_d = 5$: 152 torr, 500 RPM,$-\overline{u}_{in} = 7.4cm/sec$, $MCP_d = 7$: 180 torr, 423 RPM,$-\overline{u}_{in} = 6.3cm/sec$, $MCP_d = 10$: 215 torr, 354 RPM,$-\overline{u}_{in} = 5.2cm/sec$, $MCP_d = 15$: 263 torr, 289 RPM,$-\overline{u}_{in} = 4.3cm/sec$.

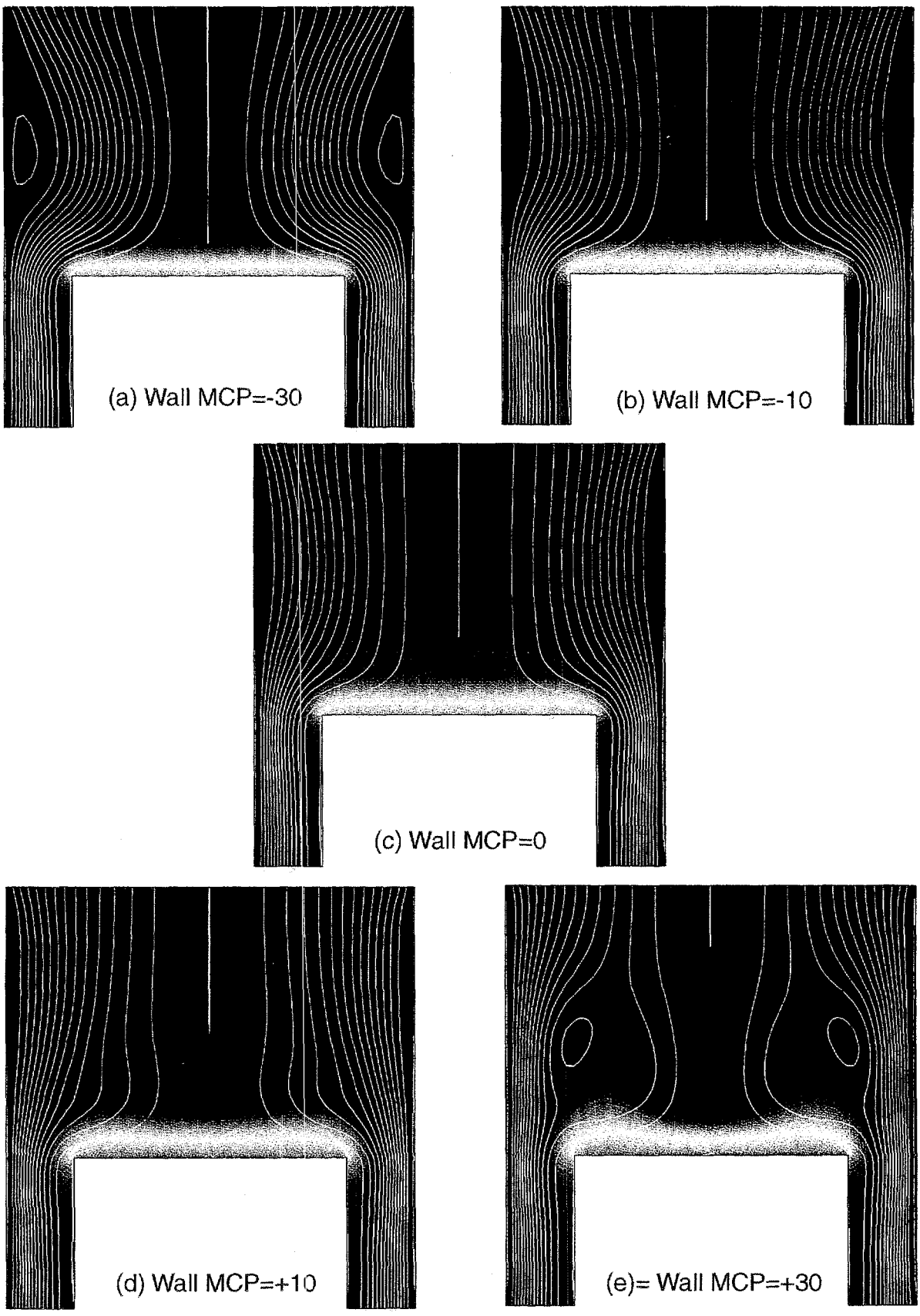

Figure 10: Influence of MCP_w on flow and temperature at $Re_\omega = 314.5$ and $MCP_d = 5$. Conditions: 27 torr, 281 RPM, $-\overline{u}_{in} = 13.2$cm/sec, $\overline{T}_d = 1300$K, $\overline{T}_{in} = 400$K, and $\overline{q}_{1D} = 3.37 \times 10^6$ergs/sec $-$ cm^2; (a) $\overline{T}_w = 479$K, (b) $\overline{T}_w = 426$K, (c) $\overline{T}_w = 400$K, (d) $\overline{T}_w = 374$K, (e) $\overline{T}_w = 321$K

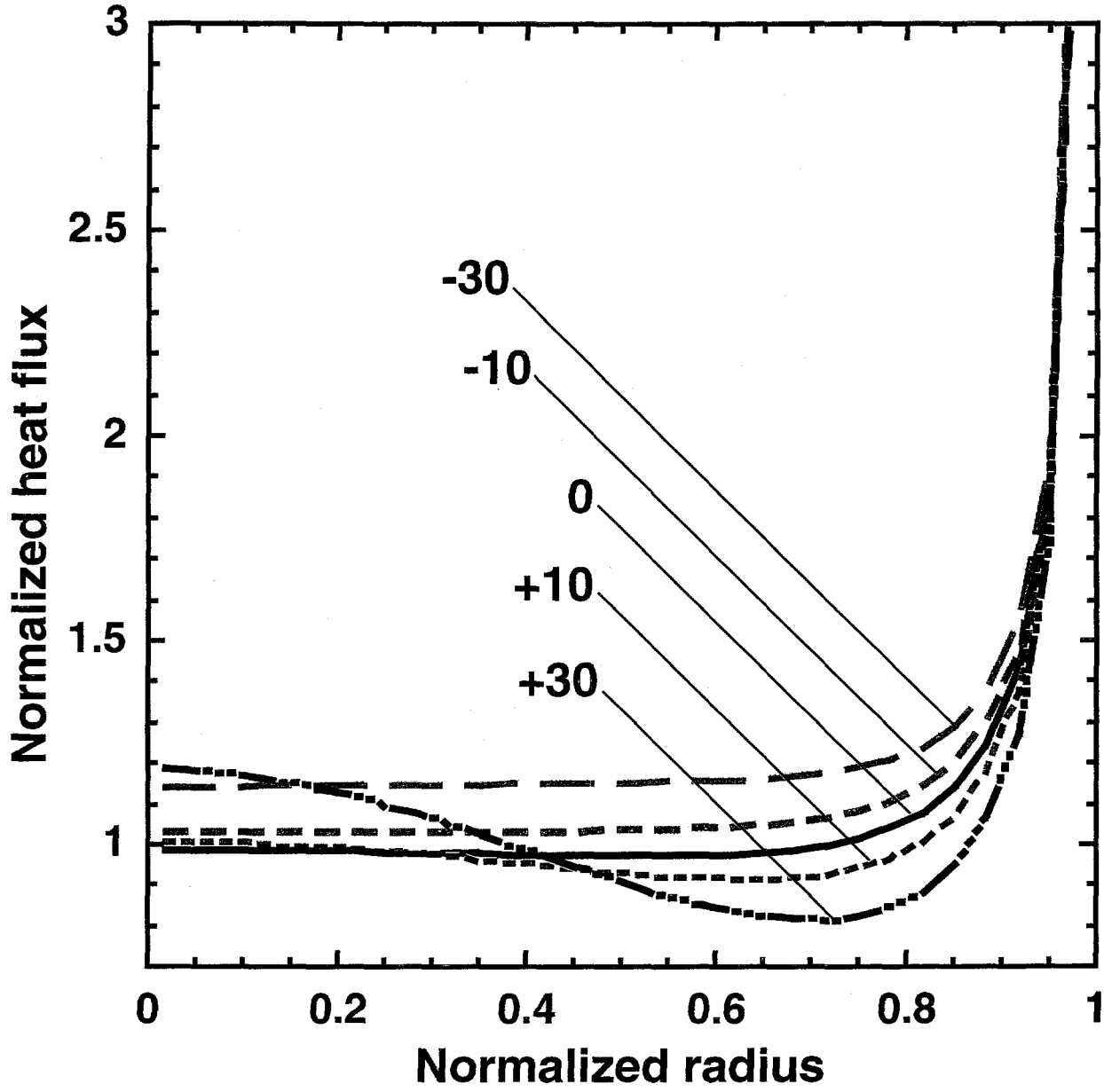

Figure 11: Influence of MCP_w on disk heat flux at $Re_\omega = 314.5$ and $MCP_d = 5$. Conditions: 27 torr, 281 RPM, $-\overline{u}_{in} = 13.2cm/sec$, $\overline{T}_d = 1300K$, $\overline{T}_{in} = 400K$, and $\overline{q}_{1D} = 3.37 \times 10^6 ergs/sec - cm^2$; $MCP_w = -30$: $\overline{T}_w = 479K$, $MCP_w = -10$: $\overline{T}_w = 426K$, $MCP_w = 0$: $\overline{T}_w = 400K$, $MCP_w = +10$: $\overline{T}_w = 374K$ $MCP_w = +30$: $\overline{T}_w = 321K$

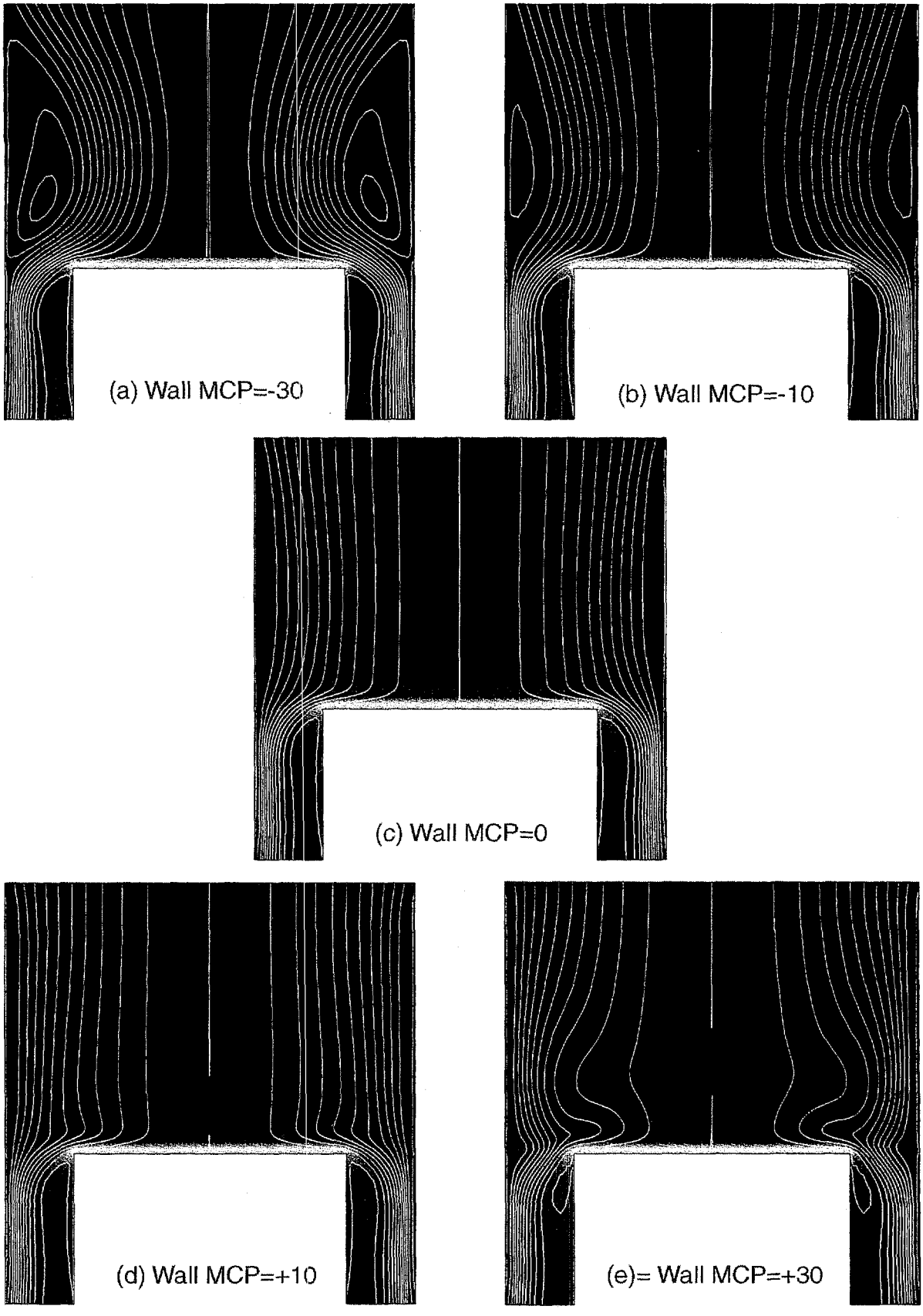

Figure 12: Influence of MCP_w on flow and temperature at $Re_\omega = 3145$ and $MCP_d = 5$. Conditions: 152 torr, 500 RPM, $-\overline{u}_{in} = 7.4$cm/sec, $\overline{T}_d = 1300$K, $\overline{T}_{in} = 400$K, and $\overline{q}_{1D} = 1.07 \times 10^7 \text{ergs/sec} - \text{cm}^2$; (a) $\overline{T}_w = 424$K, (b) $\overline{T}_w = 406$K, (c) $\overline{T}_w = 400$K, (d) $\overline{T}_w = 392$K, (e) $\overline{T}_w = 376$K

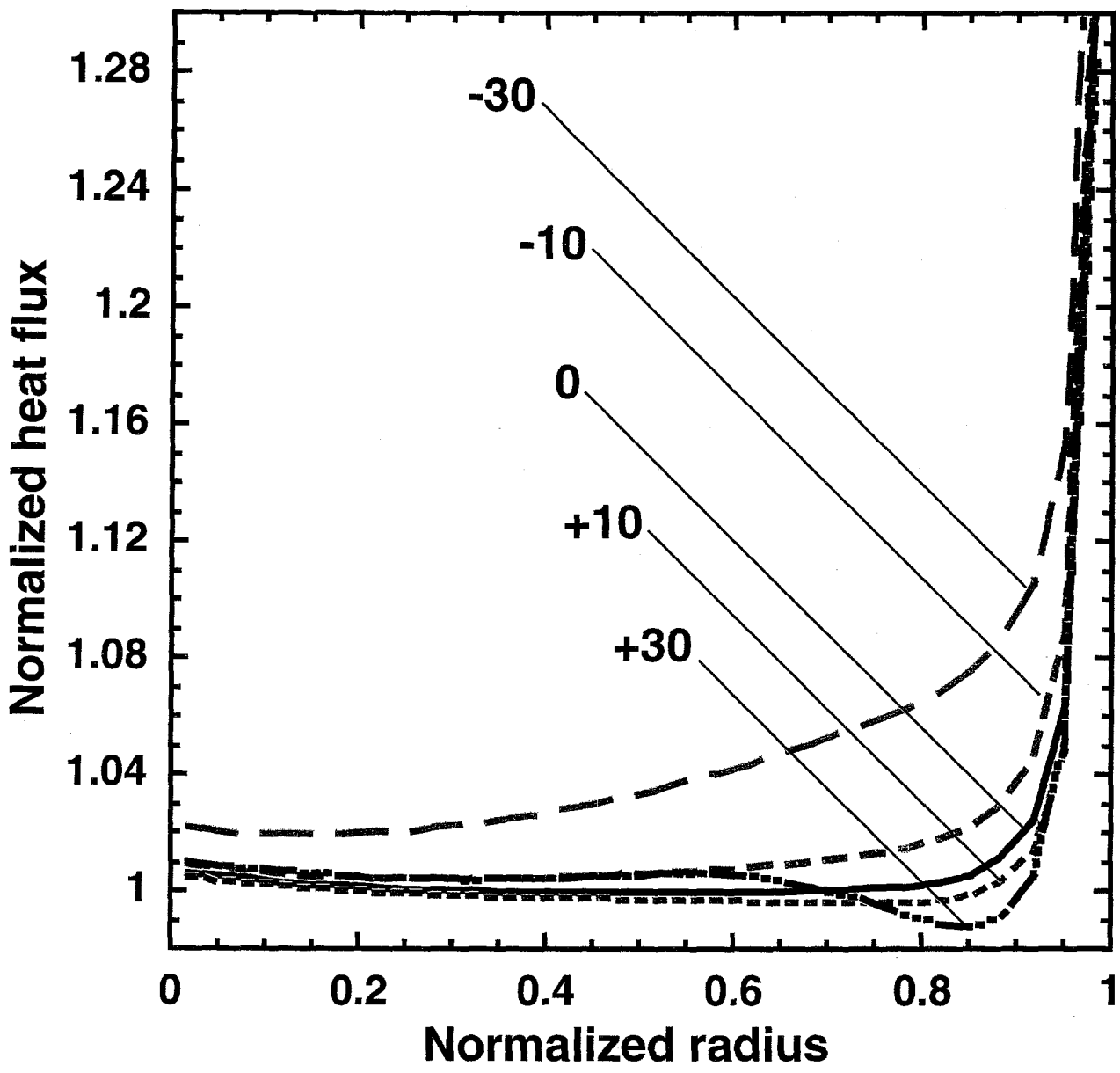

Figure 13: Influence of MCP_w on disk heat flux at $Re_\omega = 3145$ and $MCP_d = 5$. Conditions: 152 torr, 500 RPM, $-\overline{u}_{in} = 7.4$cm/sec, $\overline{T}_d = 1300$K, $\overline{T}_{in} = 400$K, and $\overline{q}_{1D} = 1.07 \times 10^7 \mathrm{ergs/sec - cm^2}$; $MCP_w = -30$: $\overline{T}_w = 424$K, $MCP_w = -10$: $\overline{T}_w = 406$K, $MCP_w = 0$: $\overline{T}_w = 400$K, $MCP_w = +10$: $\overline{T}_w = 392$K, $MCP_w = +30$: $\overline{T}_w = 376$K

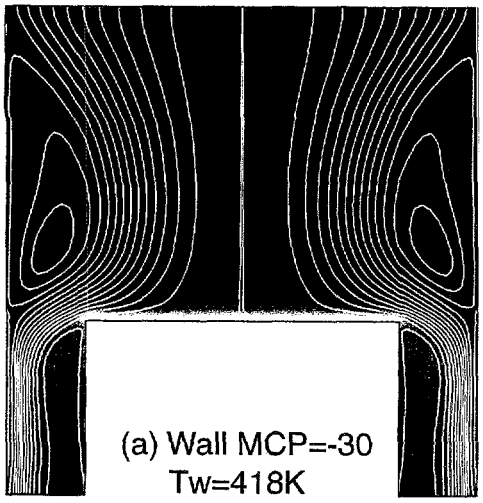

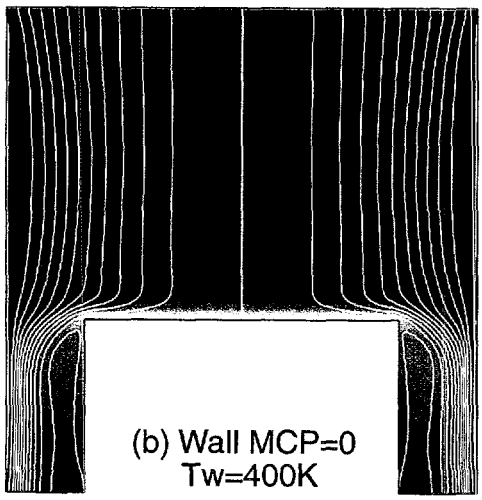

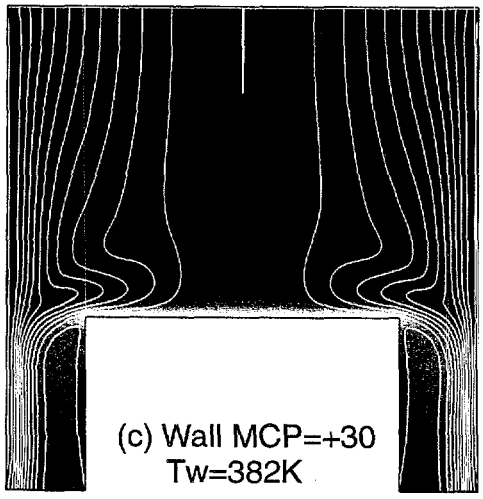

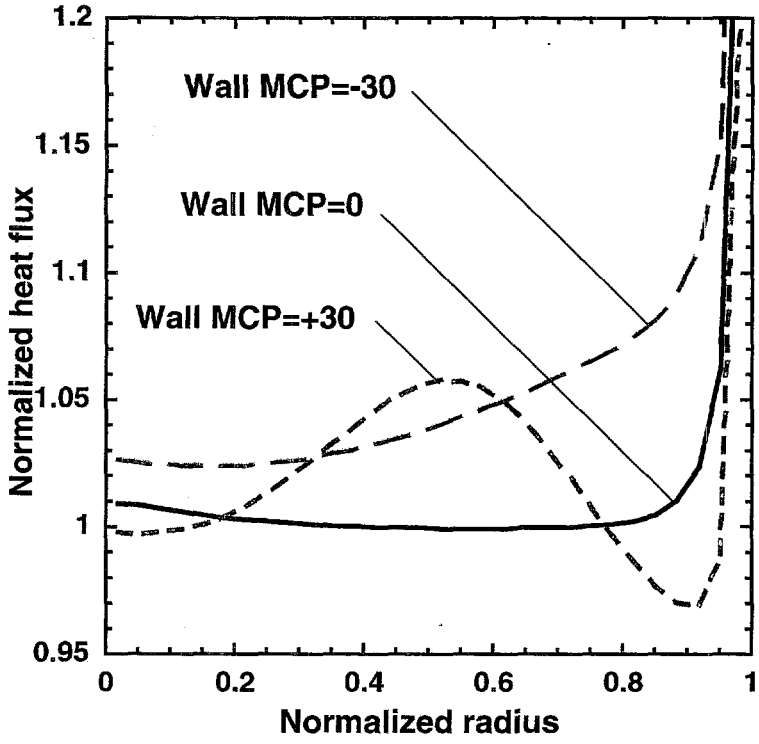

(d) Disk heat flux distribution

Figure 14: Influence of MCP_w at $Re_\omega = 3145$ and $MCP_d = 7$. Conditions: 180 torr, 423 RPM, $-\overline{u}_{in} = 6.3$cm/sec, $\overline{T}_d = 1300$K, $\overline{T}_{in} = 400$K, and $\overline{q}_{1D} = 1.07 \times 10^7$ergs/sec $-$ cm^2

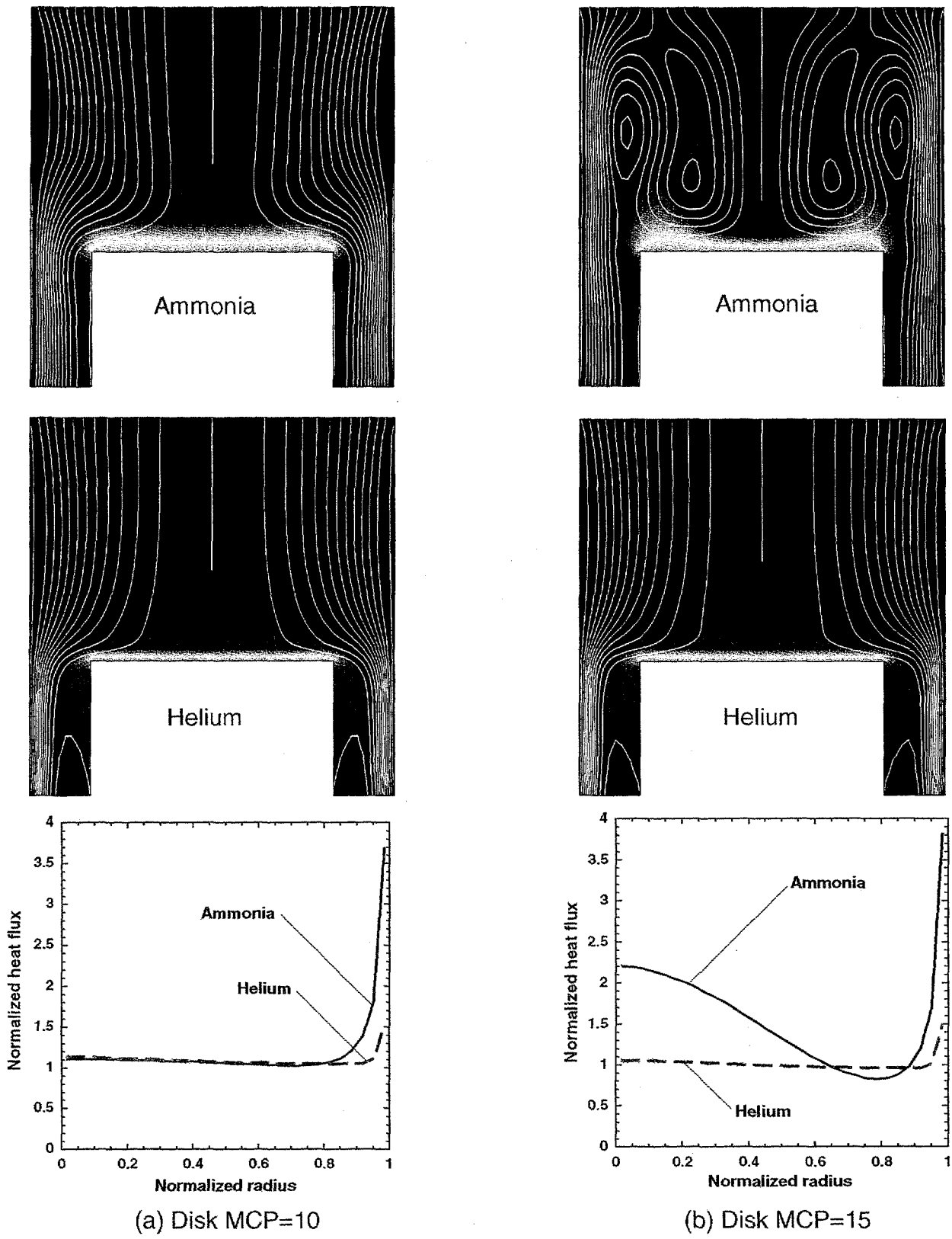

Figure 15: Influence of transport properties at $Re_\omega = 314.5$ for $MCP_w = 0$ and $MCP_d = 10$ and 15. (a) NH_3 conditions: 38.2 torr, 199 RPM, $-\overline{u}_{in} = 9.3$cm/sec, $\overline{T}_d = 1300$K, $\overline{T}_{in} = 400$K, $\overline{T}_w = 400$K and $\overline{q}_{1D} = 3.37 \times 10^6$ergs/sec $-$ cm^2; He conditions: 277 torr, 199 RPM, $-\overline{u}_{in} = 8.4$cm/sec, $\overline{T}_d = 1300$K, $\overline{T}_{in} = 400$K, $\overline{T}_w = 400$K and $\overline{q}_{1D} = 8.79 \times 10^6$ergs/sec $-$ cm^2 (b) NH_3 conditions: 46.7 torr, 162 RPM, $-\overline{u}_{in} = 7.6$cm/sec, $\overline{T}_d = 1300$K, $\overline{T}_{in} = 400$K, $\overline{T}_w = 400$K and $\overline{q}_{1D} = 3.37 \times 10^6$ergs/sec $-$ cm^2; He conditions: 277 torr, 163 RPM, $-\overline{u}_{in} = 6.8$cm/sec, $\overline{T}_d = 1300$K, $\overline{T}_{in} = 400$K, $\overline{T}_w = 400$K and $\overline{q}_{1D} = 8.79 \times 10^6$ergs/sec $-$ cm^2

References

[1] G.H. Evans and R. Greif. "Forced Flow Near a Heated Rotating Disk: A Similarity Solution". *Numerical Heat Transfer*, **14**:373–387, 1988.

[2] W. G. Breiland and G.H. Evans. "Design and Verification of Nearly Ideal Flow and Heat Transfer in a Rotating Disk Chemical Vapor Deposition Reactor". *Journal of the Electrochemical Society*, **138**(6), 1991.

[3] G.H. Evans and R. Greif. "A Numerical Model of the Flow and Heat Transfer in a Rotating Disk Chemical Vapor Deposition Reactor". *Journal of Heat Transfer*, **109**:928–935, 1987.

[4] G.H. Evans and R. Greif. "Effects of Boundary Conditions the Flow and Heat Transfer in a Rotating Disk Chemical Vapor Deposition Reactor". *Numerical Heat Transfer*, **12**:243–252, 1987.

[5] S. Patnaik, R. A. Brown, and C. A. Wang. "Hydrodynamic Dispersion in Rotating Disk OMVPE Reactors: Numerical Simulation and Experimental Measurements". *Journal of Crystal Growth*, **96**:153–174, 1989.

[6] D. Fotiadis, S. Kieda, and K. Jensen. "Transport Phenomena in Vertical Reactors for Metalorganic vapor phase epitaxy -I. Effects of Heat Transfer Characterists, Reactor Geometry, and Operating Conditions". *Journal of Crystal Growth*, **102**:441–470, 1990.

[7] F. Chou and S. Gong. "Effect of Wall Cooling on the Flow Regime Map in a Rotating-Disk CVD Reactor". *Journal of Chemical Deposition*, **3**:47–64, 1994.

[8] S.C. Palmateer, S.H. Groves, C.A. Wang, D.W. Weyburne, and R.A. Brown. "Use of Flow Visualization and Tracer Gas Studies for designing an INP/InGaAsP OMVPE Reactor". *Journal of Crystal Growth*, **83**:202–210, 1987.

[9] W.S. Winters, G.H. Evans, and R. Greif. "Mixed Binary Convection in a Rotating Disk Chemical Vapor Deposition Reactor". *International Journal of Heat and Mass Transfer*, **40**(3):737–744, 1997.

[10] W.S. Winters, G.H. Evans, and R. Greif. "A Two-Dimensional Numerical Model of Gas Mixing and Deposition in a Rotating Disk CVD Reactor". eds. T.M. Besmann, M.D. Allendorf, McD. Robinson, and R.K. Ulrich, editors, *CVD XIII, Proceedings of the Thirteenth International Conference on Chemical Vapor Deposition*, pp. 89–94, The Electrochemical Society, Pennington, NJ. 1996.

[11] F.M. White. *Viscous Fluid Flow.* McGraw-Hill, New York, NY, 1974.

[12] S.V. Patankar. *Numerical Heat Transfer and Fluid Flow.* McGraw-Hill, New York, NY, 1980.

[13] W.S. Winters, G.H. Evans, and C.D. Moen. "CURRENT - A Computer Code for Modeling Two-Dimensional, Chemically Reacting, Low Mach Number Flows". Technical Report SAND97–8202, Sandia National Laboratories, Livermore, CA, October 1996.

[14] M.E. Coltrin, R.J. Kee, G.H. Evans, E. Meeks, F.M. Rupley, and J.F. Grcar. "SPIN(version 3.83): A Fortran Program, for Modeling One-Dimensional Rotating-Disk/Stagnation-Flow Chemical Vapor Deposition Reactors". Technical Report SAND91-8003, Sandia National Laboratories, Livermore, CA, August 1991.

[15] R.J. Kee, G. Dixon Lewis, J. Warnatz, M.E. Coltrin, and J.A. Miller. "A Fortran Computer Code Package for the Evaluation of Gas-Phase Multicomponent Transport Properties". Technical Report SAND86–8246, Sandia National Laboratories, Livermore, CA, September 1991.

[16] R.J. Kee, F.M. Rupley, E. Meeks, and J.A. Miller. "Chemkin-III: A Fortran Chemical Kinetics Package for the Analysis of Gas Phase Chemical and Plasma Kinetics". Technical Report SAND96-8216, Sandia National Laboratories, Livermore, CA, May 1996.

UNLIMITED RELEASE
INITIAL DISTRIBUTION

EXTERNAL DISTRIBUTION:

Prof. T. Cale
ERC 175
Chemical/Bio & Materials Eng.
Arizona State University
Tempe, AZ 85287-6006

Prof. D. S. Dandy
Colorado State University
Dept. Agriculture and Chem Eng.
Fort Collins, 80523

Prof. H. A. Dwyer
Dept of Aero. and Mech. Eng.
University of California
Davis, CA 95616

Prof. D. L. Flamm
Dept. EECS
187M Cory Hall
University of California
Berkeley,CA 94596.

P. Gadgil
Genus, Inc.
1139 Karlstad Drive
Sunnyvale, CA 94089

R. Geels
SDL, Inc.
80 Rose Orchard Way
San Jose, CA 95134-1365

Prof. D. Goodwin
Mail Code 104-44
Mech. Eng. & Applied Physics
California Institute of Technology
Pasadena, CA 91125

S. A. Gokoglu
Lewis Research Center, MS 106-1
NASA
Cleveland, OH 44135

Prof. R. Greif
Dept. of Mech. Eng.
University of California
Berkeley, CA 94720

Prof. K. F. Jensen
Dept. Chem. Eng. MIT 66-566
Massachusetts Institute of Technology
Cambridge, Mass 02139-4307

S. Joh
Novellus Systems, Inc.
3970 N. 1st St.
M/S 251
San Jose, CA 95134

Prof. R. J. Kee
Engineering Division
Colorado School of Mines
Golden, CO 80401-1887

Prof. C. R. Kleijn
Delft University of Technology
Kramers Laboratorium voor Fysische Technologie
Prins Bernhardlaan 6, 2628 BW Delft
The Netherlands

H. Liu
Hewlett Packard
370 W. Trimble Road, MS 91MJ
San Jose, CA. 95131-1008

M. Meyyappan
Mail Stop 229-3
Ames Research Center
Moffett Field, CA 94035-1000

Prof. D. Rosner
Chemical Engineering Dept.
Yale
P.O. Box 2159 YS
New Haven, CT 06520

R. Stall
Emcore, Corporation
35 Elizabeth Avenue
Somerset, NJ 08873

P. Zawadzki
Emcore, Corporation
35 Elizabeth Avenue
Somerset, NJ 08873

INTERNAL DISTRIBUTION:

MS 0601	1126	W. G. Breiland
MS 0601	1126	M. E. Coltrin
MS 0601	1126	H. K. Moffat
MS 0601	1126	J. Y. Tsao
MS 0603	1314	P. Esherick
MS 9001	8000	T. Hunter
		Attn: J. B. Wright, 2200
		M. E. John, 8100
		A. L. West
		R. C. Wayne, 8400
		P. N. Smith, 8500
		P. E. Brewer, 8800
		D. L. Crawford, 8900
MS 9409	8250	R. H. Stulen
MS 9054	8300	W. J. Mclean
		Attn: L. A. Rahn, 8351
		D. R. Hardesty, 8361
		R. W. Carling, 8362
		R. J. Gallager, 8366
MS 9052	8361	M. D. Allendorf
MS 9053	8362	S. R. Vosen
MS 9042	8345	C. W. Hartwig
MS 9042	8345	G. H. Evans (5)
MS 9042	8345	J. F. Grcar
MS 9042	8345	S. Griffiths
MS 9042	8345	W. G. Houf
MS 9042	8345	R. S. Larson
MS 9042	8345	A. E. Lutz
MS 9042	8345	E. Meeks
MS 9042	8345	C. D. Moen
MS 9042	8345	B. Nilson
MS 9042	8345	F. Rupley
MS 9042	8345	P. Spence
MS 9042	8345	A. Ting
MS 9042	8345	W. S. Winters (10)

MS 9405	8700	M. T. Dyer
		Attn: M. W. Perra, 8711
		M. I. Baskes, 8712
		J. C. F. Wang, 8713
		K. L. Wilson, 8716
		W. G. Wolfer, 8717
		T. Chen, 8742
		P. E. Nielan, 8743
MS 9405	8743	L. A. Bertram
MS 9405	8743	D. R. Chenoweth
MS 9405	8743	M. P. Kanouff
MS 0841	9100	P. L. Hommert
MS 0833	9103	J. H. Biffle
MS 0826	9111	W. L. Hermina
		Attn: D. K. Gartling, 9111
		R. Shunk, 9111
MS 0826	9111	S. Kempka
MS 0834	9112	A. C. Ratzel
		Attn: M. R. Baer
		M. Martinez
MS 0835	9113	B. Blackwell
MS 0835	9113	R. Cochran
MS 0834	9114	A. S. Geller
MS 0836	9116	C. W. Peterson
MS 0836	9116	S. R. Tieszen
MS 1111	9221	S. S. Dosanjh
		Attn: J. N. Shadid
		A. G. Salinger

MS 9021	Technical Communications Dept., 8815, for OSTI (2)
MS 9021	Technical Communications Dept., 8815/Technical Library, MS 0899, 4916
MS 0899	Technical Library, 4916 (4)
MS 9018	Central Technical Files, 8940-2 (3)